An Open Loop Guidance Architecture for Navigationally Robust On-Orbit Docking

Hung-Sheng Chern

An Open Loop Guidance Architecture for Navigationally Robust On-Orbit Docking

Hung-Sheng Chern
The George Washington University
Joint Institute for Advancement of Flight Sciences
Langley Research Center • Hampton, Virginia

Abstract

The development of an open-loop guidance architecture is outlined for autonomous rendezvous and docking (AR&D) missions to determine whether the Global Positioning System (GPS) can be used in place of optical sensors for relative initial position determination of the chase vehicle. Feasible command trajectories for one, two, and three impulse AR&D maneuvers are determined using constrained trajectory optimization. Early AR&D command trajectory results suggest that docking accuracies are most sensitive to vertical position errors at the initial condition of the chase vehicle. Thus, a feasible command trajectory is based on maximizing the size of the locus of initial vertical positions for which a fixed sequence of impulses will translate the chase vehicle into the target while satisfying docking accuracy requirements. Documented accuracies are used to determine whether relative GPS can achieve the vertical position error requirements of the impulsive command trajectories. Preliminary development of a thruster management system for the Cargo Transfer Vehicle (CTV) based on optimal throttle settings is presented to complete the guidance architecture. Results show that a guidance architecture based on a two impulse maneuver generated the best performance in terms of initial position error and total velocity change for the chase vehicle.

Contents

List of Figures

viii

List of Tables

Nomenclature

x	in-plane horizontal distance component for Cartesian coordinate system
y	in-plane vertical distance component for Cartesian coordinate system
y_e	point of occurance for maximum value of q(y)
Δt	total transfer time, sec
ΔV	total velocity change of the chase vehicle, in/s
ΔV_0	total velocity of the chase vehicle associated with the initial impulse, in/s
ΔV_i	total velocity of the chase vehicle associated with the second impulse, in/s
ΔV_{ii}	total velocity of the chase vehicle associated with the third impulse, in/s
δ	variational operator
$\vec{\lambda}$	Lagrange multiplier vector
ω	orbital angular velocity, rad/s
Φ_{in}	in-plane state transition matrix
θ	in-plane angular sweep in polar coordinate system
$\mathcal{Y}_0$	locus of initial chase vehicle vertical positions, ft
Δy_0	admissible initial vertical error, in
$\mathcal{F}_1, \mathcal{F}_2, \mathcal{F}_3$	set of free parameters for one, two, and three impulse maneuvers, respectively
t	time, sec
x_{gate}	horizontal position of gate constraint, ft
y_{gate}	vertical position of gate constraint, ft
y_{targ}	vertical position tolerance at target, in
v_{targ}	maximum docking speed, in/s

Subscripts

0	at initial position
f	at final time
gate	at gate geometry
i	at second impulse
ii	at third impulse
targ	at target vehicle
$time_1$	time constraint relation for two impulse command trajectories
$time_2$	time constraint relation for three impulse command trajectories

Superscripts

$\cdot$	derivative with respect to time
$\rightarrow$	vector

Acronyms

AR&D	autonomous rendezvous and docking
CTV	cargo transfer vehicle
DOF	degree-of-freedom
EP	explorer platform
GPS	global positioning system
H.O.T.	higher-order terms
IMU	inertial measurement unit
LaRC	Langley Research Center
LEO	low-Earth orbit
MSFC	Marshall Space Flight Center
NASA	National Aeronautics and Space Administration
NAVSTAR	navigation system using timing and ranging
TOPEX	ocean topography experiment

Chapter 1

Introduction

Present rendezvous and docking procedures for the U.S. space program have relied heavily upon crew and ground involvement. The most taxing of all the phases in a rendezvous and docking mission is arguably the terminal phase of the rendezvous. Under present conditions, the pilot operations take precedence over nearly all the on-board guidance and navigation. The terminal approach is performed manually using visual cues and proximity data from extremely accurate sensors. However, rendezvous systems of this type are highly susceptible to pilot error and, considering the cost and complexity of the subsystems required, are expensive to perform on a regular basis.

The future of the space program include plans for rendezvous and docking missions such as satellite servicing and unmanned cargo resupply of Space Station Freedom. Thus, the development of a reliable autonomous rendezvous and docking maneuver is an integral step for progress in the space program. The foundation for a reliable AR&D maneuver is a navigational system which can accurately provide relative position and velocity throughout the entire docking procedure.

1.1   Types of Rendezvous Maneuvers

There exist two different types of terminal phase rendezvous maneuvers - docking and berthing maneuvers. In general, both types of procedures involve the maneuvering of a chase vehicle to meet a target vehicle in orbit so that the two vehicles can couple,

presumably for purposes of mass transfer. Specifically, docking refer to maneuvers in which the chase vehicle flies directly into the target with a nonzero final velocity [1]. Berthing maneuvers refer to the use of an intermediate device, such as a manipulator arm, to grapple the chase vehicle as it is brought to a relative standstill near the target [1]. Thus, berthing maneuvers do not require a closing velocity between the two vehicles. While docking maneuvers provide the simplest means of coupling two vehicles in orbit, they do introduce some risk in the areas of collision, guidance, navigation, and control.

1.2   Current Sensor Technology

Some of the most common sensors used to determine relative position are visual sensors and laser navigation sensors. These sensors are used since they can obtain the highly stringent accuracy requirements associated with terminal phase rendezvous and docking maneuvers. Visual sensors, such as video-only cameras and sophisticated automatic pattern recognition cameras [2], are susceptible to adverse lighting conditions and require high computer throughput [3]. Laser navigation systems require the placement of reflectors on the target. Thus, a highly accurate knowledge of the reflector location relative to the target vehicle coordinate system is required. This essentially means that a complete knowledge of the target vehicle attitude is necessary for an accurate laser measurement.

Both systems essentially require a direct line-of-sight between the chase and target vehicle. This partially accounts for the so-called R-bar and V-bar terminal approaches associated with current rendezvous and docking procedures in which the chase vehicle flies directly towards the target along the radial or tangential directions, respectively.

While these two conventional navigation systems have provided adequate results for present rendezvous and docking missions, future autonomous rendezvous and docking (AR&D) missions, particular for unmanned vehicles, require a system that provides sufficiently accurate results while, at the same time, is not restricted by some of the limitations of visual sensors and laser navigation.

1.3 Global Positioning System Overview

The Global Positioning System (GPS) is a constellation of navigation satellites and is a means of providing the U.S. military with accurate latitude, longitude, altitude, travel velocity, and time under any environmental conditions. This system was initially proposed in the 1970's with the first Navigation System using Timing And Ranging (NAVSTAR) GPS satellite launched in 1978 [4]. The present constellation consists of 24 satellite positions at an altitude of 10,924 nmi, with four satellites at each of the six 55 deg inclined equally spaced orbital planes [5].

GPS technology has developed to the point where it is now a means of providing an ideal on-board precision navigation and pointing capability for Low Earth Orbit (LEO) missions [6]. In fact, several flight experiments have been proposed which incorporate the use of GPS position and attitude determination for AR&D missions. One such proposed flight demonstration suggests an AR&D mission between a small, low-cost, NASA satellite powered by batteries and a cold gas thruster and the Explorer Platform (EP) Spacecraft. Under this proposed scenario, the sensor system is comprised of a GPS receiver, a laser illuminator, and a video camera. The GPS receiver is used for both absolute and relative positioning for coarse guidance of up to 330 ft while the laser illuminator and the video camera are used for fine guidance [7].

However, relative GPS position determination has improved to the point where inch accuracies are possible. Recent precision orbit determination experiments with the Ocean Topography Experiment (TOPEX)/Poseidon satellite have obtained radial ephemeris RMS difference accuracies to within 1.18 - 1.57 inches [8]. Ground surveying experiments using relative GPS have also obtained inch accuracies in relative position determination [9].

However, these accuracies are based on GPS data transmitted through the atmosphere. Thus, these accuracies can be affected by tropospheric delays, ionospheric delays, and multipath errors due to ground structures. In this study, it is conceivable that relative GPS accuracies between orbiting vehicles are much better than those

3

previously documented. Recent evaluations of relative GPS position determination for AR&D missions has shown that it is theoretically possible to obtain relative position accuracies to within 0.394 inches [10]. Thus, it may be possible to replace optical sensors with relative GPS as a cheaper means of navigation.

1.4 Scope of Investigation

The scope of this investigation is to develop an open-loop guidance architecture for the terminal phase of an AR&D mission to determine whether relative GPS can be used in place of optical sensors. Figure (1.1) illustrates a schematic of the open-loop system.
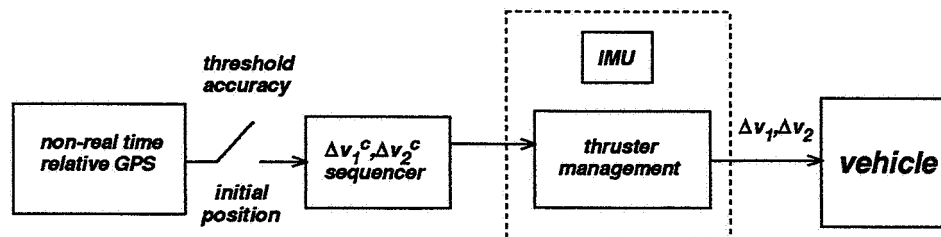
Figure 1.1: Open-loop guidance architecture

The first step in the open-loop system is the use of non-real time relative GPS to determine the initial position of the chase and target vehicles. Once the threshold accuracy for the relative position between the vehicles is achieved, the chase vehicle is given a fixed sequence of pre-determined ΔV commands. The final step in the open-loop process is the execution of the commands from the ΔV sequencer by the thruster management system. In addition to the firing laws, the thruster management system includes an inertial measurement unit (IMU). Thruster management laws can be affected by errors that are cause by finite burn-time effects and thruster errors. For short periods, the IMU would be used to correct these errors. The development of the guidance architecture is done in two steps. First, feasible command trajectories are determined for one, two, and three impulse maneuvers. Second, a thruster management system is developed to execute these command trajectories.

1.4.1   Feasible Command Trajectories

In this study, feasible command trajectories govern the fixed sequences of impulses. These trajectories are determined for one, two, and three impulse AR&D maneuvers. Previous impulsive guidance research suggests that accuracies at docking are most sensitive to vertical position errors at the initial condition of the chase vehicle and is rather insensitive to horizontal position errors (see Appendix A). Thus, command trajectories are determined by using optimization methods to maximize the range of admissible initial vertical position errors of the chase vehicle. The maximized admissible vertical position errors for each of the command trajectories are compared to navigational accuracies attainable through relative GPS to determine whether it is a viable maneuver. Chapter 2 outlines the vehicle model, mission parameters, and mission constraints. Chapters 3, 4, and 5 detail the optimization formulation and command trajectory results for the various impulse maneuvers.

5

1.4.2 Thruster Management System

The approach in developing the thruster management system is to determine optimal throttle settings for the chase vehicle thrusters to realize the impulse commands for the feasible command trajectories. A modulator is then required to determine minimum firing times based on these optimal throttle settings. This study presents the preliminary design of the thruster management system by developing the formulations to determine these optimal throttle settings. Chapter 6 outlines the specific chase vehicle thruster model and the basic optimization formulations.

Chapter 2

Mission Description

This chapter presents the basic assumptions for the mission, the vehicle model, the mission parameters, and the mission constraints for the terminal phase AR&D maneuver.

2.1 Basic Assumptions

There are several basic assumptions which govern the type of AR&D maneuver determined by the command trajectories. First, it is assumed that the chase vehicle is on-orbit with the target and trails the target by some given distance, say 600 ft. While in its initial position, the chase vehicle is assumed to have no relative motion with respect to the target. Also, the docking mechanism is assumed to be located on the far side of the target vehicle. This requires an AR&D maneuver where the chase vehicle must fly to the front of the target vehicle to complete the docking mission. Finally, to obtain the highest degree of relative position accuracy using relative GPS, issues such as integer ambiguity and cycle slip are assumed to be resolved.

2.2 Vehicle Model

Several assumptions are made concerning the vehicle model. Since this study involves the terminal phase of an AR&D maneuver, equations are determined which govern

the motion of the chase vehicle relative to the target vehicle for small perturbations about a reference orbit. In this case, the reference orbit is assumed to be the circular orbit of the target vehicle. This naturally assumes that the radial component of the target velocity does not change with respect to time and with respect to the orbital position. Conversely, if the reference orbit had a slight eccentricity, such an assumption concerning the radial velocity component of the target vehicle would not be true. Furthermore, the orbital angular velocity of the target vehicle, ω, is also assumed to be constant. Thus, the transfer angle between the chase and target vehicle is simply the product of the angular velocity and the transfer time Δt.

The dynamical model and coordinate system for the rendezvous and docking mission are constituted by the Clohessy-Wiltshire equations [11]. This is a Cartesian coordinate system centered on a target assumed to be in a circular orbit and involves linear time-invariant dynamics. The Clohessy-Wiltshire equations are also known as Hill's equations and have been used to analyze the relative motion of two satellites in orbit in close proximity to each other. The model presented in this report represent the motion in the vertical plane. The geometry is shown in Fig. (2.1). The target-centered Cartesian coordinate system is orientated such that the y-axis is always pointing radially outward from the center of the Earth and the x-axis is pointing in the opposite direction of the target vehicle velocity vector. In this representation, the x and y-axes are in the orbit plane.

For the target-centered coordinate system, the in-plane linearized equations of relative motion for the chase vehicle are [11]

$$\left.\begin{array}{c} \ddot{x} - 2\omega\dot{y} = 0 \\ \ddot{y} - 3\omega^2 y + 2\omega\dot{x} = 0 \end{array}\right\} \tag{2.1}$$
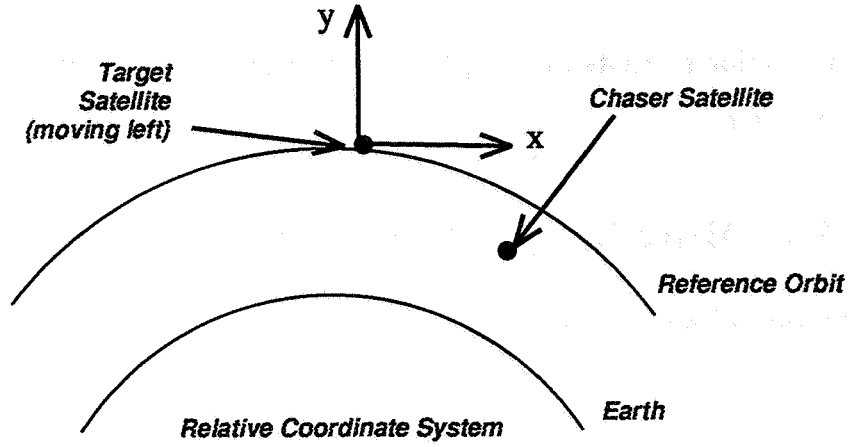
Figure 2.1: Coordinate system geometry

The solution to Eqn. (2.1) results in an in-plane chase vehicle motion governed by [11]

$$
\begin{bmatrix} x(\Delta t) \\ y(\Delta t) \\ \dot{x}(\Delta t) \\ \dot{y}(\Delta t) \end{bmatrix} = \Phi_{in}(\Delta t) \begin{bmatrix} x_0 \\ y_0 \\ \dot{x}_0 \\ \dot{y}_0 \end{bmatrix}
\tag{2.2}
$$

where

$$
\Phi_{in}(\Delta t) = \begin{bmatrix} 1 & 6(\omega \Delta t - \sin \omega \Delta t) & \frac{4}{\omega} \sin \omega \Delta t - 3\Delta t & \frac{2}{\omega}(1 - \cos \omega \Delta t) \\ 0 & 4 - 3\cos \omega \Delta t & \frac{-2}{\omega}(1 - \cos \omega \Delta t) & \frac{1}{\omega} \sin \omega \Delta t \\ 0 & 6\omega(1 - \cos \omega \Delta t) & 4\cos \omega \Delta t - 3 & 2\sin \omega \Delta t \\ 0 & 3\omega \sin \omega \Delta t & -2\sin \omega \Delta t & \cos \omega \Delta t \end{bmatrix}
\tag{2.3}
$$

Equation (2.2) is a state transition expression for the chase vehicle dynamics based on its initial position, x_0 and y_0, velocity, $\dot{x}_0$ and $\dot{y}_0$, and a transfer time, Δt.

9

2.3 Mission Constraints

This section presents the target accuracy requirements of the AR&D mission and the motivation behind and the requirements of the gate constraints.

2.3.1 Basic Target Constraints

The orbital altitude, h, of the target vehicle is approximately 255 mi. Table (2.1) lists the allowable position and velocity tolerances at the target for the chase vehicle. For this particular AR&D problem, the chase vehicle must be within a vertical (y-axis) accuracy of ± 0.591 in and a maximum speed tolerance of 0.591 in/s (priv. communication - Mr. Fred Roe, MSFC - April 30, 1993). These constraints assume that the chase vehicle motion is restricted to the orbital plane.

Table 2.1: Target accuracy requirements

	Category	Accuracy
	Vertical target tolerance - y_{targ}	0.591 in
Target	Maximum allowable speed - v_{targ}	0.591 in/s

With the docking accuracies set, the target constraints for the constrained optimization problem which must be satisfied by the chase vehicle are represented as

$$
\mathcal{C}_{targ} = \begin{cases}
x(t_{targ}) &= 0 \\
y(t_{targ}) &\leq y_{targ} \\
y(t_{targ}) &\geq -y_{targ} \\
\dot{x}^2(t_{targ}) + \dot{y}^2(t_{targ}) &\leq v_{targ}^2
\end{cases}
\tag{2.4}
$$

where $y_{targ} > 0$. The first of Eqn. (2.4) requires that the chase vehicle physically docks with the target at the transfer time of t_{targ}. The remainder of Eqn. (2.4) are the vertical position tolerance and the maximum speed tolerance summarized in Table (2.1).

2.3.2 Additional Constraints

Previously unpublished work has been done for this type of impulsive AR&D command trajectory. Appendix A outlines the basic formulation and presents some basic results for this early AR&D research. In summary, the early AR&D results suggests two points. First, accuracy at docking seems most sensitive to the initial vertical position errors of the chase vehicle. Second, early simulation results show that, with just target constraints, optimized trajectories for the chase vehicle tend to approach the target tangentially. While handling vertical position sensitivity is presented later in this work, the simulation results shown in Fig. (A.2) justify the need for additional chase vehicle constraints to generate a more direct and predictable final approach towards the target vehicle.

For this particular problem, it is assumed that the target docking port is facing the same direction as the target vehicle velocity vector. Thus, the command trajectory for the chase vehicle must approach the target from the negative x-axis. While any docking approach could have been chosen, this particular type of approach takes advantage of the target vehicle velocity. Recall that the target motion is in the negative x-axis direction. A final approach trajectory from that direction requires less total velocity change by the chase vehicle. To generate such a trajectory, a gate constraint placed at an arbitrary position ahead of the target is added to the optimization problem. Figure (2.2) displays the desired final approach trajectory for the chase vehicle. The exact position of the gate geometry relative to the target is listed in Table (2.2). While these particular parameters are arbitrarily chosen, an appropriate gate position for actual flight experiments would be highly dependent upon the configuration of the chase and target vehicles. The gate position must be chosen such that the docking procedure does not result in any collisions between possible extended appendages present in the vehicle configurations. Note that the illustration in Fig. (2.2) is not drawn to scale.

11
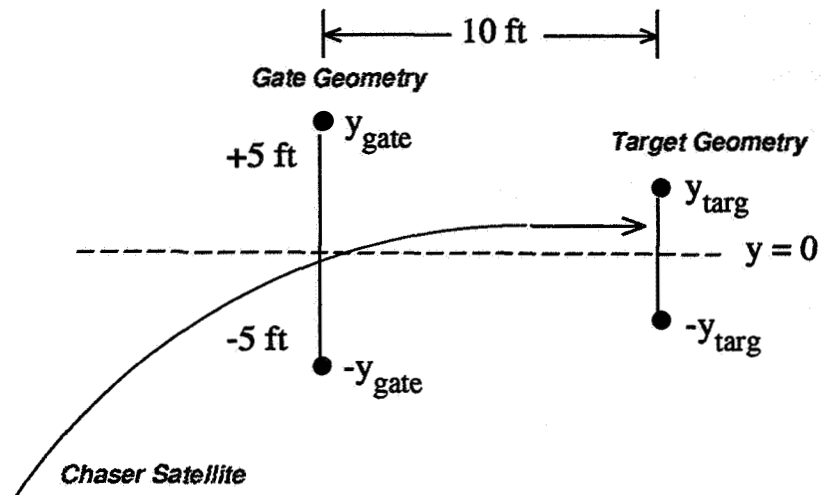
Figure 2.2: Maneuver constraints geometry

Table 2.2: Gate constraint position

	Category	Accuracy
Gate	Vertical gate tolerance - y_{gate}	$5ft$
	Horizontal gate position - x_{gate}	$-10ft$

Based on this trajectory approach requirement, the gate constraints for the chase vehicle are represented as

$$
\mathcal{C}_{gate} = \begin{cases}
\dot{x}(t_{gate}) & \geq & 0 \\
x(t_{gate}) & = & x_{gate} \\
y(t_{gate}) & \leq & y_{gate} \\
y(t_{gate}) & \geq & -y_{gate}
\end{cases}
\tag{2.5}
$$

where $y_{gate} > 0$. The first portion of Eqn. (2.5) is the mathematical representation that the chase vehicle must eventually approach the target from the negative x-axis direction at the transfer time of t_{gate}. The remaining portions of Eqn. (2.5) are just the geometric constraints listed in Table (2.2).

As a final assurance that the approach trajectory is from the negative x-axis direction, an additional constraint must be added to Eqn. (2.4). Equation (2.6) controls the horizontal component of the chase vehicle velocity at the target insuring that the final chase vehicle motion is in the positive x-axis direction.

$$
\dot{x}(t_{targ}) \geq 0
\tag{2.6}
$$

To completely quantify this final approach trajectory, Eqn. (2.6) must be added to the target constraints. Thus, the complete target constraints for the constrained optimization problem are expressed as

$$
\mathcal{C}_{targ} = \begin{cases}
x(t_{targ}) & = & 0 \\
\dot{x}(t_{targ}) & \geq & 0 \\
y(t_{targ}) & \leq & +y_{targ} \\
y(t_{targ}) & \geq & -y_{targ} \\
\dot{x}^2(t_{targ}) + \dot{y}^2(t_{targ}) & \leq & v_{targ}^2
\end{cases}
\tag{2.7}
$$

13

Chapter 3

Single Impulse AR&D Maneuver

This chapter develops a single impulse command trajectory. The single impulse command trajectory is determined by maximizing the locus of initial vertical positions for which a single impulse translates the chase vehicle into the target while satisfying all gate and target constraint conditions outlined in Chapter 2. This locus of vertical positions is expressed as

$$\mathcal{Y}_0 = \{y = y_0 + \delta y, |\delta y| \leq \Delta y_0\} \tag{3.1}$$

The scalar cost function for the AR&D trajectory optimization is, accordingly,

$$\mathcal{J} = \Delta y_0 \tag{3.2}$$

where $\Delta y_0 > 0$. For each command trajectory, the free parameters of the problem are x_0, y_0, Δy_0, $\dot{x}_0$, $\dot{y}_0$, $(t_{targ})_y$, and $(t_{gate})_y$. The parameters $(t_{targ})_y$ and $(t_{gate})_y$ correspond to target and gate times for different trajectories emanating from (x_0, y) where $y \in \mathcal{Y}_0$. In the results generated for the single impulse command trajectories, the parameter x_0 is selected by the user. To simplify the notation, the set of free parameters for each trajectory in the single impulse maneuver is expressed as

$$\mathcal{F}_1(y) = \{y, (t_{targ})_y, (t_{gate})_y, \dot{x}_0, \dot{y}_0 \, ; \, x_0\} \tag{3.3}$$

While results are presented for the single impulse AR&D command trajectories, the initial portion of this chapter illustrate the individual steps taken in the research to mathematically determine this locus of admissible initial vertical positions for the chase vehicle.

3.1 Constrained Trajectories

While maximizing Δy_0 provides a means of determining this locus of initial vertical positions, no mention has yet been made on how to represent Δy_0. In this section, the steps taken in the research are presented individually to show how a set of constrained trajectories are used to quantify Δy_0. These constrained trajectories are actual optimized trajectories of the chase vehicle which satisfy gate and target constraints of Eqns. (2.5) and (2.7), respectively.

3.1.1 Two Trajectory Formulation

A straightforward method of maximizing Δy_0 is to use a two trajectory approach. In this method, determining the uppermost ($\delta y > 0$) and lowermost ($\delta y < 0$) vertical trajectories about the nominal initial chase vehicle position, x_0 and y_0, will in essence determine the maximum Δy_0. Thus, for a given x_0, the maximum admissible vertical position error is determined by maximizing Eqn. (3.2) subject to two sets of gate and target constraints, i.e.

$$\left. \begin{array}{l} \mathcal{C}_{targ}(\mathcal{F}_1(y_0 + \Delta y_0)) \\ \mathcal{C}_{targ}(\mathcal{F}_1(y_0 - \Delta y_0)) \\ \mathcal{C}_{gate}(\mathcal{F}_1(y_0 + \Delta y_0)) \\ \mathcal{C}_{gate}(\mathcal{F}_1(y_0 - \Delta y_0)) \end{array} \right\} \tag{3.4}$$

where $\mathcal{C}_{targ}$ and $\mathcal{C}_{gate}$ are represented in Eqns. (2.7) and (2.5), respectively. Two sets of gate and target constraints are needed since two trajectories are propagated towards the target and each of these trajectories must satisfy all constraints.

However, one issue associated with this approach is that it assumes all the intermediate trajectories for the chase vehicle emanating from $y \in \mathcal{Y}_0$ satisfy gate and target constraints. To test this assumption, an optimization routine is performed based on Eqns. (3.2) and (3.4) at $x_0 = 600$ ft. All constraints are determined as a function of initial vertical position. Unfortunately, the interior trajectories do not satisfy all gate and target constraints as is assumed. In fact, only one constraint is not satisfied. Figure (3.1) graphically represents the target constraint relation

$$e_y(\Delta y_0) = y(t_{targ}) - y_{targ} \leq 0 \tag{3.5}$$

Physically, this represents the difference between the final chase vehicle vertical position and the maximum vertical position target tolerance. For fully satisfied interior trajectories, this constraint value must be less than zero, but as can be seen from Fig. (3.1), this is not the case.
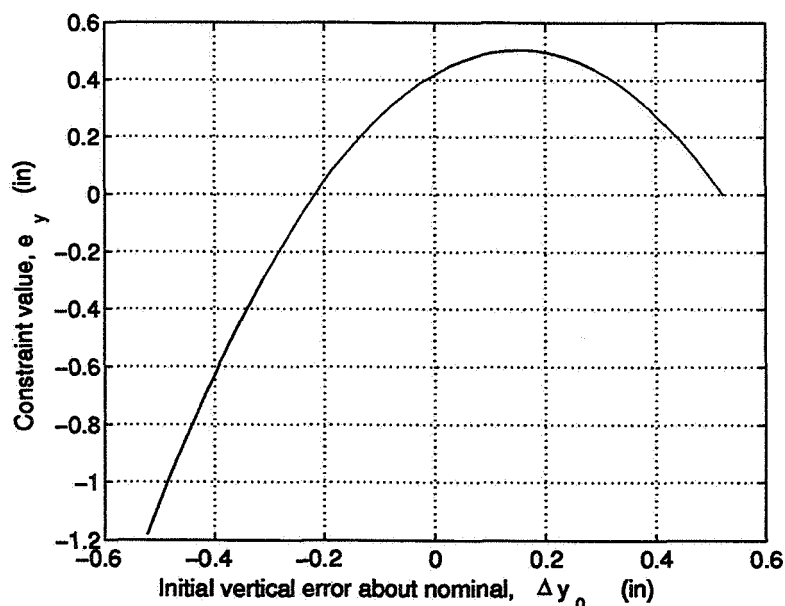
Figure 3.1: Maximum vertical tolerance target constraint for the chase vehicle

3.1.2 Three Trajectory Formulation

Since interior trajectories do not satisfy constraints, any solution obtained from such a formulation is unreliable. However, the problem at hand is still to maximize the locus of initial vertical positions for the chase vehicle. Thus, the optimization routine must be reformulated so that all interior trajectories do in fact satisfy gate and target constraints.

A seemingly simple solution to this problem is to add a third middle trajectory to the formulation. This additional middle trajectory can act to constrain the behavior of e_y such that it is satisfied for all interior trajectories. While the original cost function is still valid, an additional set of gate and target constraints is applied to this third trajectory. The modified problem statement is to maximize Eqn. (3.2) subject to Eqn. (3.4) and, additionally,

$$\left. \begin{array}{c} \mathcal{C}_{targ}(\mathcal{F}_1(y_0)) \\ \mathcal{C}_{gate}(\mathcal{F}_1(y_0)) \end{array} \right\} \qquad (3.6)$$

This modified problem statement still, however, assumes that all interior trajectories, in addition to the three already specified, satisfy all gate and target constraints. Figure (3.2) illustrates the same constraint relation as in Fig. (3.1) with the additional results stemming from the three trajectory formulation.

Figure (3.2) does illustrate the fact that including an additional trajectory to the problem statement almost satisfies Eqn. (3.5). While a majority of all possible interior trajectories do satisfy gate and target constraints, a small portion still do not satisfy the problem formulation assumption.

17
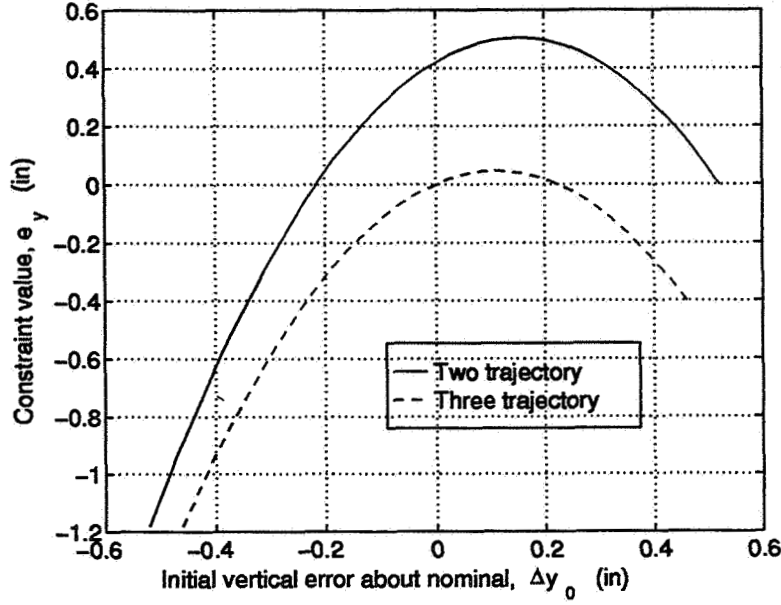
Figure 3.2: Vertical tolerance constraint comparison between two trajectory and three trajectory formulations

3.1.3 Quadratic-Fit Formulation

Visual examination of Fig. (3.2) suggests that it may be possible to control the entire constraint behavior by taking advantage of what appears to be a parabolic relationship in Eqn. (3.5). By using the individual constraint values obtained from the three trajectory formulation, a quadratic relation between these values and the initial relative vertical position of the chase vehicle can be determined using Lagrange's interpolating polynomials. Using this quadratic model, the constraint behavior in Eqn. (3.5) can be controlled to be less than or equal to zero by forcing the quadratic to be less than or equal to zero at its maximum point.

Lagrange Interpolating Polynomials

The first step in this process is to determine the coefficients for the Lagrange interpolating polynomial. Equations (3.7) and (3.8) represent the general formulation for an nth order Lagrange interpolating polynomial [12]:

$$L_{n,k}(x) = \prod_{i=0}^{n} \frac{(x - x_i)}{(x_k - x_i)} \tag{3.7}$$

$$P(x) = \sum_{k=0}^{n} f(x_k) L_{n,k}(x) \tag{3.8}$$

where $i \neq k$ and x_i and $f(x_i)$ are the given data points and corresponding function values, respectively.

However, this particular problem only involves a second-order interpolating polynomial. Thus, Eqns. (3.7) and (3.8) can be reduced to

$$\left. \begin{aligned} L_0(x) &= \frac{(x-x_1)(x-x_2)}{(x_0-x_1)(x_0-x_2)} \\ L_1(x) &= \frac{(x-x_0)(x-x_2)}{(x_1-x_0)(x_1-x_2)} \\ L_2(x) &= \frac{(x-x_0)(x-x_1)}{(x_2-x_0)(x_2-x_1)} \end{aligned} \right\} \tag{3.9}$$

$$P(x) = f(x_0)L_0(x) + f(x_1)L_1(x) + f(x_2)L_2(x) \tag{3.10}$$

Equations (3.9) and (3.10) can be rearranged and expressed in the more familiar form of a second-order polynomial, i.e.

$$P(x) = D_0 x^2 + D_1 x + D_2 \tag{3.11}$$

where the polynomial coefficients are defined as

$$\left. \begin{aligned} D_0 &= (f(x_0)A_0 + f(x_1)A_1 + f(x_2)A_2) \\ D_1 &= -(f(x_0)B_0 + f(x_1)B_1 + f(x_2)B_2) \\ D_2 &= (f(x_0)C_0 + f(x_1)C_1 + f(x_2)C_2) \end{aligned} \right\} \tag{3.12}$$

$$\left. \begin{aligned} A_0 &= [(x_0 - x_1)(x_0 - x_2)]^{-1} \\ A_1 &= [(x_1 - x_0)(x_1 - x_2)]^{-1} \\ A_2 &= [(x_2 - x_0)(x_2 - x_1)]^{-1} \end{aligned} \right\} \tag{3.13}$$

$$B_0 = A_0(x_1 + x_2) \\ B_1 = A_1(x_0 + x_2) \\ B_2 = A_2(x_0 + x_1) \qquad \qquad (3.14)$$

$$C_0 = A_0 x_1 x_2 \\ C_1 = A_1 x_0 x_2 \\ C_2 = A_2 x_0 x_1 \qquad \qquad (3.15)$$

Quadratic Constraint Formulation and Results

Equations (3.11), (3.12), (3.13), (3.14), and (3.15) constitute the set of relations which are used to model the constraint behavior of Eqn. (3.5). To insure that the constraint is always satisfied, the maximum point of Eqn. (3.11) must be no greater than zero. Thus, a single constraint is added to the three trajectory optimization formulation. First, a quadratic is fit to the constraint relation behavior, i.e.

$$q(y; \ y_0 - \Delta y_0, y_0, y_0 + \Delta y_0) \ : \ \begin{cases} q(y_f(y_0 + \Delta y_0)) &= e_y(y_0 + \Delta y_0) \\ q(y_f(y_0)) &= e_y(y_0) \\ q(y_f(y_0 - \Delta y_0)) &= e_y(y_0 - \Delta y_0) \end{cases} \qquad (3.16)$$

where $q(y)$ is simply the second-order Lagrange interpolating polynomial. Equation (3.16) has a single maximum point which occurs at

$$y_e = \arg \left\{ \frac{dq}{dy}(y) = 0 \right\} \qquad \qquad (3.17)$$

Assuming that Eqn. (3.5) is sufficiently modeled by Eqn. (3.16), then the additional constraint

$$q(y_e) \le 0 \qquad \qquad (3.18)$$

is adequate for enforcing the interior trajectory constraint assumption.

Figure (3.3) compares the interior constraint relations for the various methods discussed. It appears that the quadratic model assumption for the constraint relation is valid, and by implementing the quadratic constraint, the violated constraint behavior can be control such that the interior trajectory assumption is satisfied. Figure (3.3) also illustrates that as e_y improves from the two trajectory to the three trajectory, quadratic-fit formulation, there exists an overall loss in performance, i.e. Δy_0 decreases. However, the slight loss in performance is necessary to insure the validity of the optimized solutions.
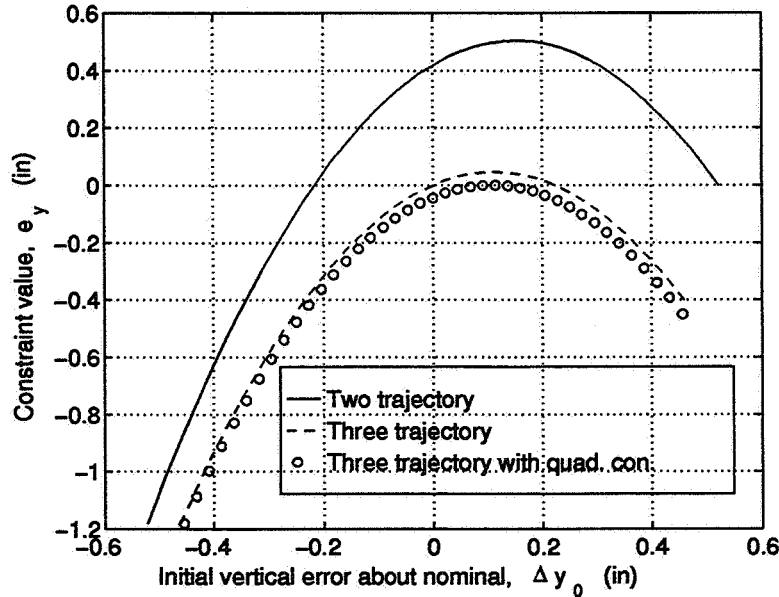
Figure 3.3: Vertical tolerance constraint comparison between two trajectory, three trajectory, and three trajectory with quadratic constraint formulations

A major assumption with the additional quadratic-fit constraint is that the constraint behavior of e_y is adequately modeled by a second-order polynomial. Appendix B summarizes the derivation for the relationship between the final and the initial chase vehicle relative vertical position. Based on typical solutions, the analytic solution shows that the relationship is in fact quadratic.

21

Formulation Summary

To maximize the locus of initial vertical position errors represented in Eqn. (3.1), the scalar cost function for the AR&D mission is expressed as Eqn. (3.2). To quantify this cost function, a constrained trajectory optimization problem is proposed based on a three trajectory, quadratic-fit formulation. In short, the constrained optimization problem is to maximized Eqn. (3.2) subject to Eqns. (3.4), (3.6), and (3.18).

3.2 Single Impulse AR&D Results

With the problem statement properly formulated, valid results can be presented for the single impulse guidance maneuver. Recall that the problem is to determine feasible command trajectories where the chase vehicle is assumed to initially start several hundred feet behind the target.

3.2.1 Optimized Results for a Single Initial Position

Figures (3.4) and (3.5) display the progression of the chase vehicle with respect to time. Figure (3.6) is a simulation of the in-plane relative position for all three optimized trajectories. Finally, Figs. (3.7) and (3.8) illustrate the early progression and the final approach, respectively, of the chase vehicle for all three trajectories. These results are based on an initial relative horizontal position, x_0, for the chase vehicle of 600 ft.

Figures (3.7) and (3.8) illustrate the quadratic behavior between the initial vertical position and the final vertical position of the chase vehicle. The lower trajectory appears to initially swing out further than the upper trajectory while the third trajectory stays the middle course. However, Fig. (3.8) displays very different results. An initial middle vertical position results in a final vertical position near the maximum position tolerance at the target. However, an initial upper vertical position results in a final vertical position very close to nominal. Lastly, an initial lower vertical position results in a final vertical position near the minimum position tolerance at the target.

The free time parameter, t_{targ}, converged to a transfer time of approximately 95 minutes which is approximately one orbital rotation. Finally, the performance, Δy_0, for this particular initial chase vehicle position is determined to have a maximum value of 0.457 in. However, this performance is based on a single initial chase vehicle position. Since initial relative horizontal position is a user-defined parameter, it is possible to generate a family of results based on this relative position. The maximum overall performance can then be determined.

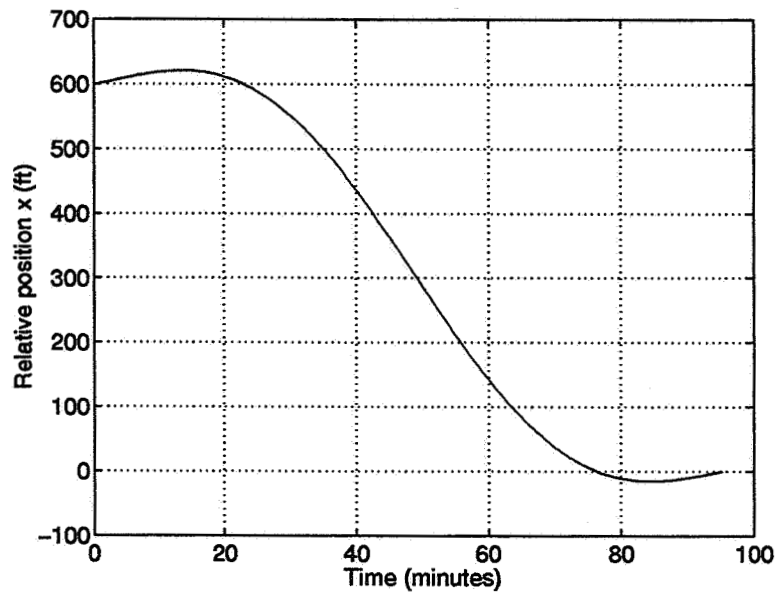Figure 3.4: Horizontal relative position for chase vehicle starting at $x_0 = 600$ ft
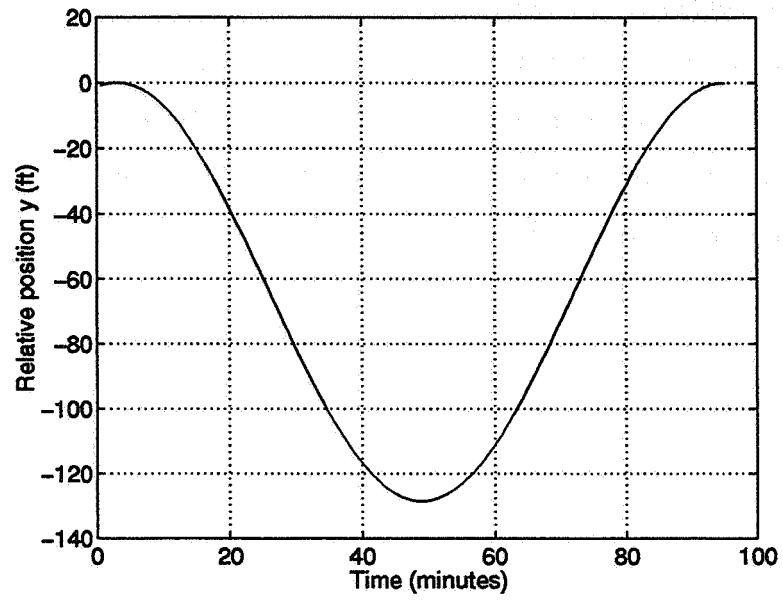
Figure 3.5: Vertical relative position for chase vehicle starting at $x_0 = 600$ ft
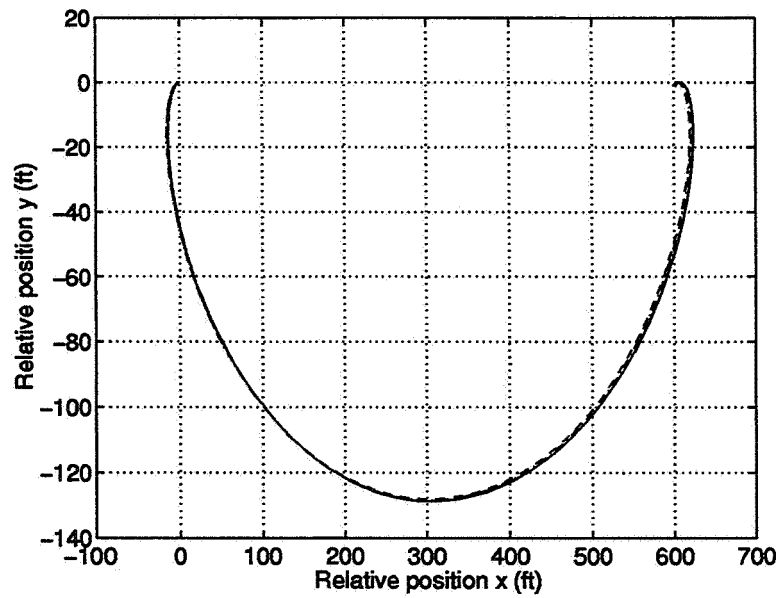
Figure 3.6: Trajectory simulation for the chase vehicle starting at $x_0 = 600$ ft

24
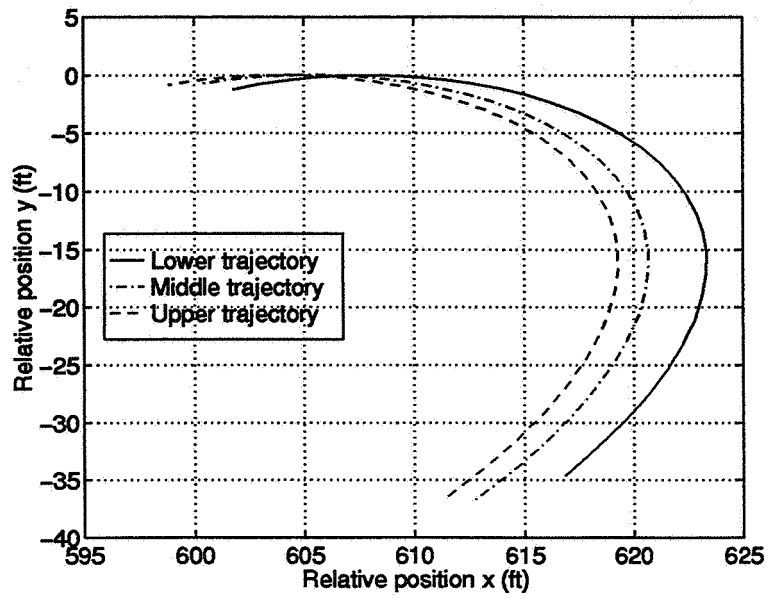
Figure 3.7: Early trajectory for the chase vehicle starting at $x_0 = 600$ ft
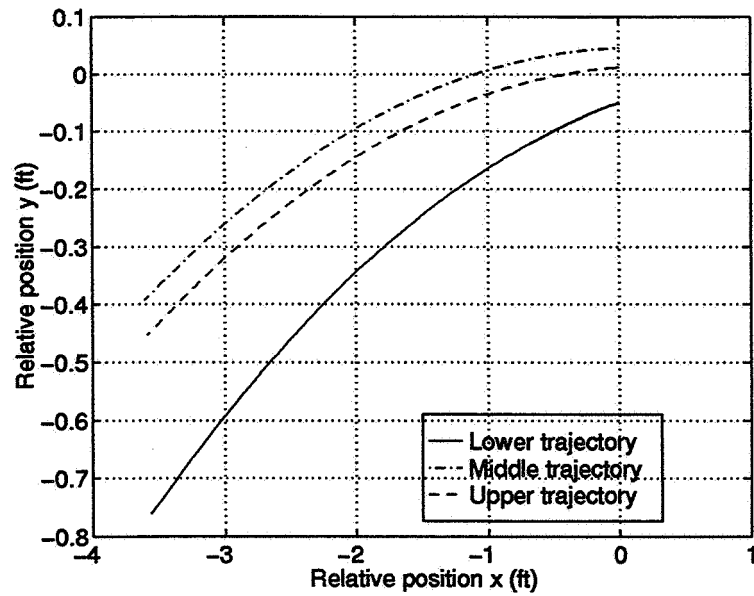
Figure 3.8: Final approach trajectory for chase vehicle starting at $x_0 = 600$ ft

3.2.2   Family of Optimized Results

By defining a range of initial relative horizontal positions, a family of results can be obtained for the single impulse command trajectory. Examining the performance trend for this family of results can be used to determine the highest overall cost value and to ascertain whether the scheme is navigationally robust to allow a successful single impulse AR&D maneuver.

Figure (3.9) displays the optimal cost of Eqn. (3.2) as a function of the initial relative chase vehicle position, x_0. Figure (3.10) depicts the corresponding variation in the impulse velocity components. Figure (3.11) is related to Fig. (3.10) in that it illustrates the impulse speed with respect to the chase vehicle's initial relative position. Finally, Fig. (3.12) depicts the chase vehicle speed at the target.

Over the range of approximately 450 ft to 825 ft, Fig. (3.9) shows that the cost function in relation with x_0 is roughly piecewise linear with a change in slope occurring at approximately $x_0 \approx 675$ ft. Also, solutions above 825 ft could not be obtained. Both phenomena are likely due to the fact that the terminal velocity constraint of the chase vehicle becomes active. From Fig. (3.12), as x_0 approaches 825 ft, the chase vehicle speed at the target approaches the maximum speed tolerance of 0.591 in/s. This terminal speed condition shown is also the reasonable cause behind the sudden drop in the vertical impulse component depicted in Fig. (3.10). The drop in the vertical impulse component balances the the gradual increase of the horizontal impulse component to 0.591 in/s.

Based on these results, the total accuracy requirement, $2\Delta y_0$, for the single impulse command trajectory at $x_0 = 600$ ft is 0.914 in. This is slightly below the range documented in relative GPS accuracy experiments [8, 9, 10]. While the accuracy requirement may be attainable, it certainly would be prudent to generate command trajectories with much more relaxed relative position accuracies between the chase and target vehicles.
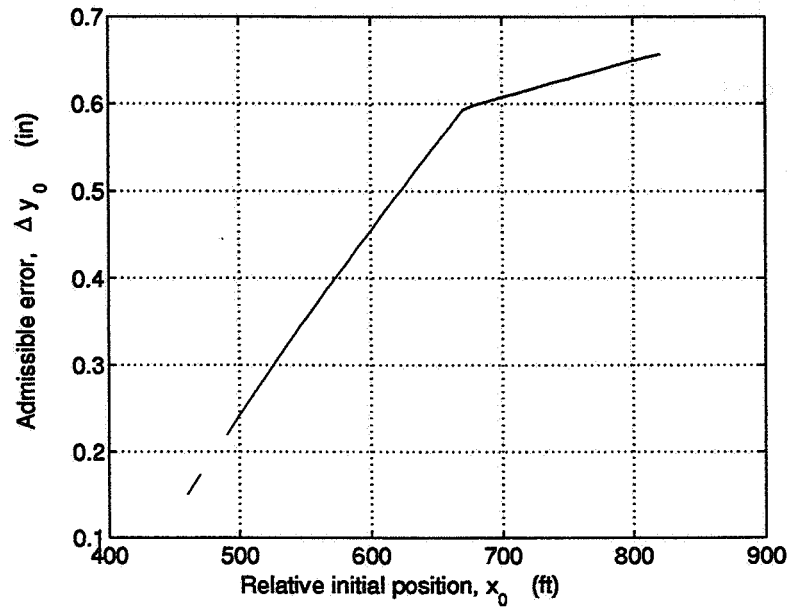
Figure 3.9: Performance robustness with respect to initial relative horizontal chase vehicle position
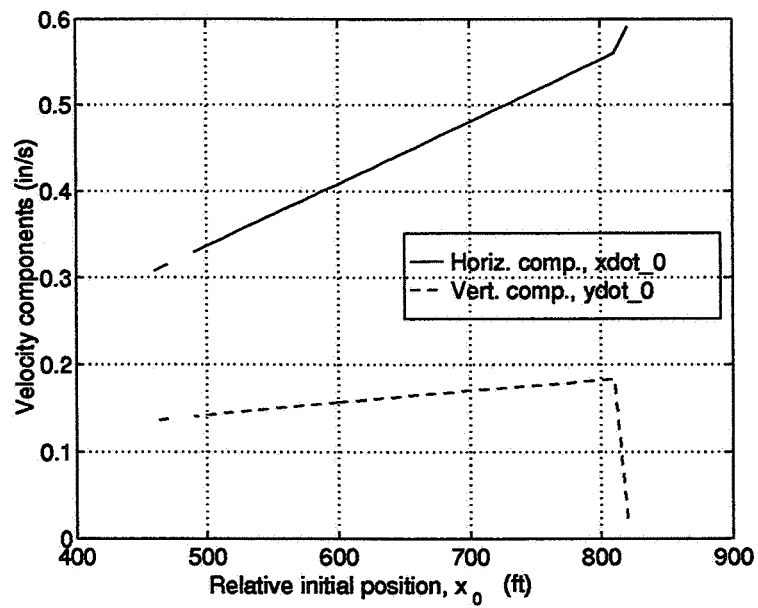
Figure 3.10: Initial impulse components with respect to initial relative horizontal chase vehicle position
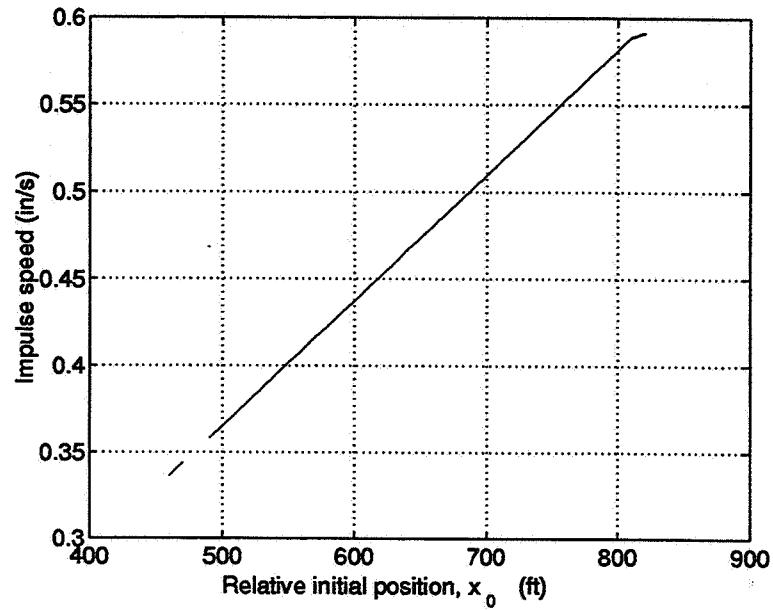
Figure 3.11: Initial impulse speed with respect to initial relative horizontal chase vehicle position
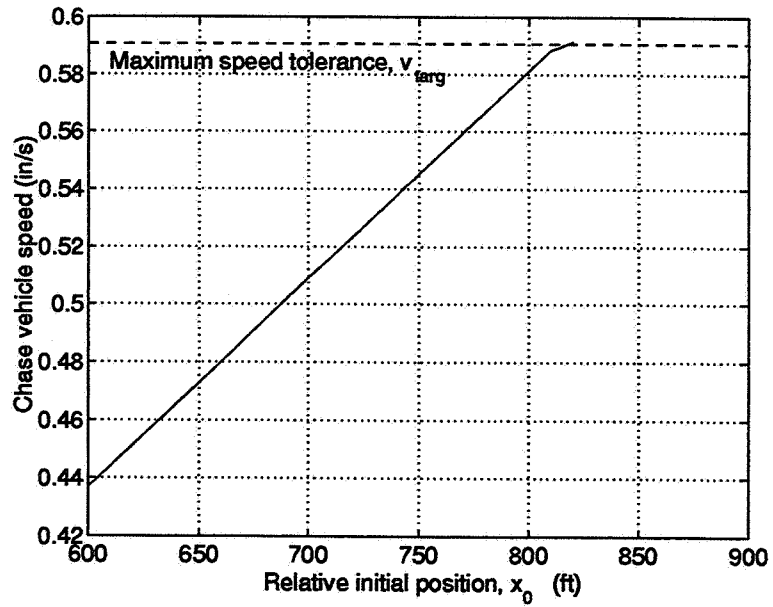
Figure 3.12: Terminal chase vehicle speed with respect to initial relative horizontal chase vehicle position

Chapter 4

Two Impulse AR&D Maneuver

The degree of vertical position accuracy required for a single impulse AR&D command trajectory is rather stringent under certain initial chase vehicle positions. It is desirable to develop a command trajectory with enough freedom to provide the required accuracy based on relative GPS position determination. With a two impulse command trajectory, up to three additional degrees-of-freedom are possible due to the parameters defining the second impulse. These additional parameters are $\dot{x}_i$, the horizontal velocity component of the second impulse, $\dot{y}_i$, the vertical velocity component of the second impulse, and t_i, the application time of the second impulse. In the results generated for the two impulse command trajectories, the parameters x_0 and t_i are selected by the user. For each constrained trajectory, the free parameters are x_0, y_0, Δy_0, $\dot{x}_0$, $\dot{y}_0$, $\dot{x}_i$, $\dot{y}_i$, t_i, $(t_{targ})_y$, and $(t_{gate})_y$. For a simpler notation, the parameters are defined as

$$\mathcal{F}_2(y) = \{y, (t_{targ})_y, (t_{gate})_y, \dot{x}_0, \dot{y}_0, \dot{x}_i, \dot{y}_i \, ; \, x_0, t_i\} \tag{4.1}$$

where $y \in \mathcal{Y}_0$ and $\mathcal{Y}_0$ is defined in Eqn. (3.1).

4.1 Optimization Formulation

The problem statement is to optimize Eqn. (3.2) subject to Eqn. (3.18) and

$$\left.\begin{array}{l} \mathcal{C}_{gate}(\mathcal{F}_2(y_0 + \Delta y_0)) \\ \mathcal{C}_{gate}(\mathcal{F}_2(y_0)) \\ \mathcal{C}_{gate}(\mathcal{F}_2(y_0 - \Delta y_0)) \\ \mathcal{C}_{targ}(\mathcal{F}_2(y_0 + \Delta y_0)) \\ \mathcal{C}_{targ}(\mathcal{F}_2(y_0)) \\ \mathcal{C}_{targ}(\mathcal{F}_2(y_0 - \Delta y_0)) \end{array}\right\} \qquad (4.2)$$

Furthermore, a constraint is added to physically insure that the firing of the second impulse occurs before the chase vehicle reaches the gate constraint, t_{gate}. This time constraint is represented as

$$\mathcal{C}_{time_1} = \left\{ \; t_i \leq t_{gate} \right. \qquad (4.3)$$

Since all three trajectories must satisfy this constraint, Eqn. (4.3) imposes the following set of constraints to the problem formulation

$$\left.\begin{array}{l} \mathcal{C}_{time_1}(\mathcal{F}_2(y_0 + \Delta y_0)) \\ \mathcal{C}_{time_1}(\mathcal{F}_2(y_0)) \\ \mathcal{C}_{time_1}(\mathcal{F}_2(y_0 - \Delta y_0)) \end{array}\right\} \qquad (4.4)$$

Another advantage of Eqn. (4.4) is that it helps to control plume contamination or plume impingement. For close proximity maneuvers between orbiting vehicles, the firing of thrusters by one vehicle can cause adverse effects in the desired relative motion with the other vehicle. In this particular problem, the target vehicle is assumed to be in a fixed position relative to the chase vehicle. A close proximity impulse firing by the chase vehicle can contaminate the assumed fixed position of the target vehicle. By requiring that the second impulse be fired at or before encountering the gate constraint, plume contamination can be controlled.

4.2 Two Impulse AR&D Results

To generate an appropriate performance comparison between the single impulse and the two impulse command trajectories, a family of results is generated where x_0 is fixed at 600 ft.

4.2.1 Optimization Results

Figure (4.1) displays the cost function variation with respect to t_i at $x_0 = 600$ ft. Figures (4.2) and (4.3) represent the initial impulse and second impulse velocity components, respectively, with respect to t_i. Figures (4.4) and (4.5) displays the variation of the individual impulse magnitudes and the total ΔV of the chase vehicle with respect to t_i.
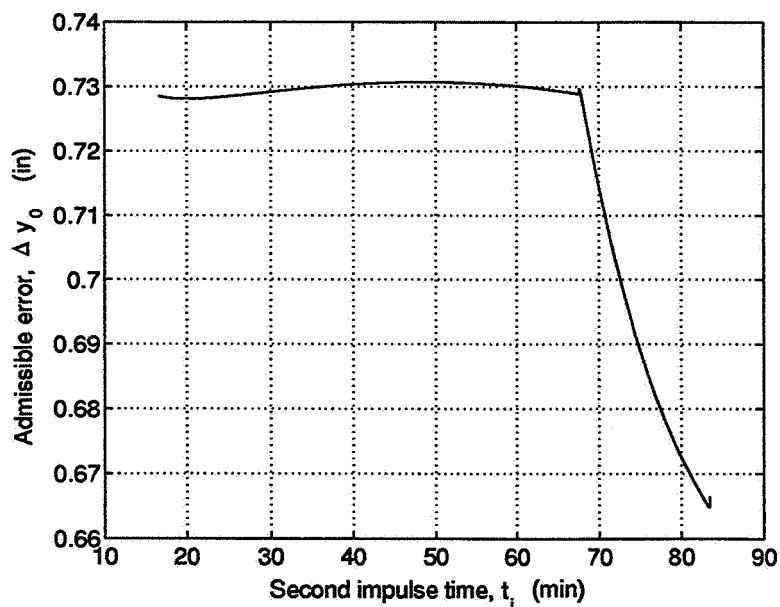
Figure 4.1: Performance robustness for two impulse maneuver at $x_0 = 600$ ft

31
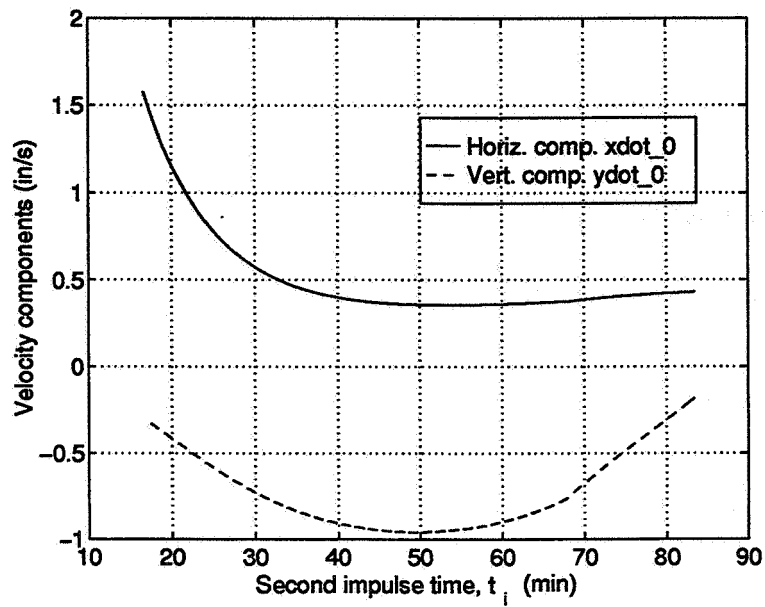
Figure 4.2: Variation of initial impulse components at $x_0 = 600$ ft
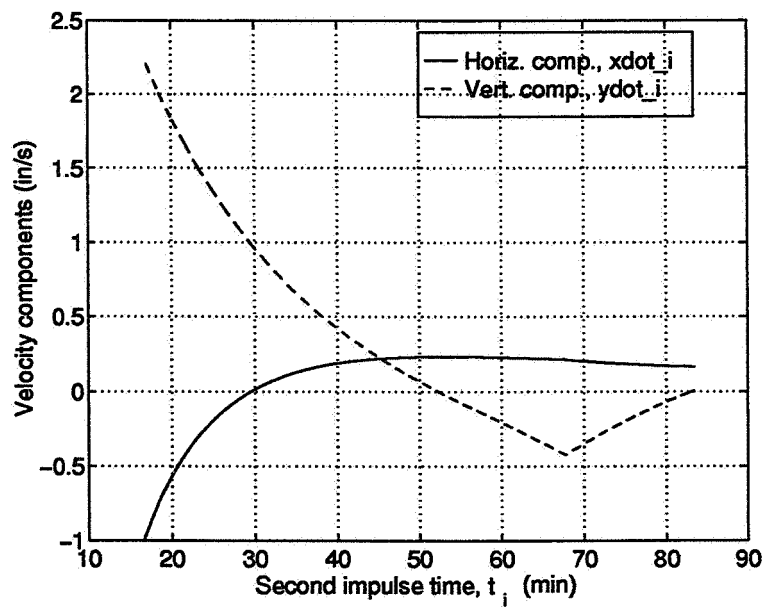
Figure 4.3: Variation of second impulse components at $x_0 = 600$ ft
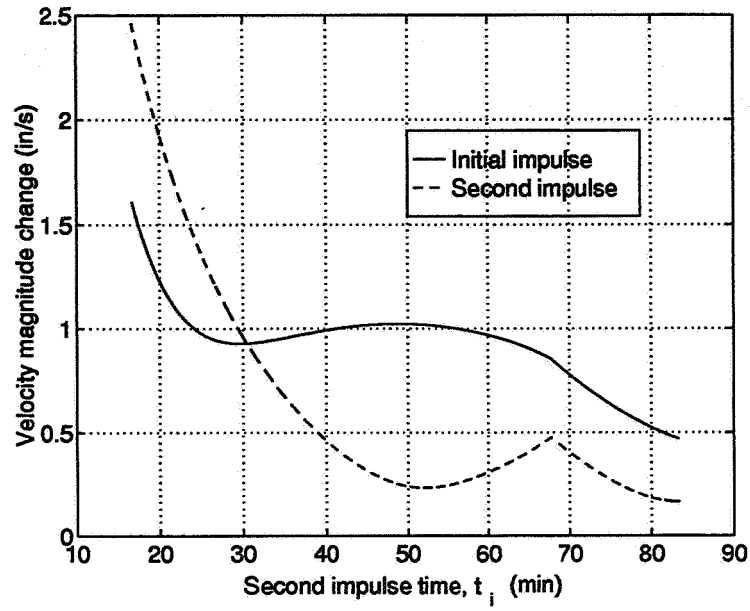
Figure 4.4: Impulse speeds with respect to second impulse time at $x_0 = 600$ ft
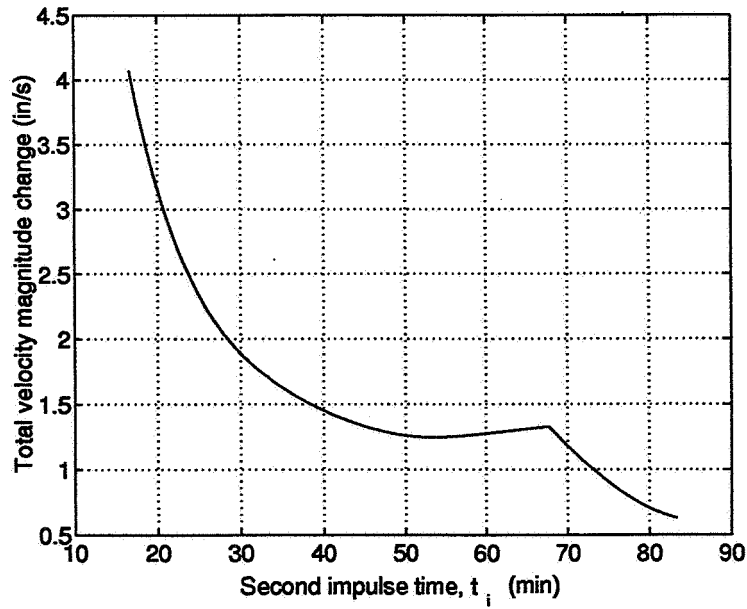
Figure 4.5: Total speed change with respect to second impulse time at $x_0 = 600$ ft

As compared to results documented in Chapter 3, two impulse command trajectories produce nearly a 60.5% increase in performance, i.e. Δy_0 increases to 0.728 in for a total required GPS accuracy of 1.46 in. In fact, Fig. (4.1) reveal that the performance remains nearly constant regardless of t_i. Figures (4.2), (4.3), (4.4), and (4.5) illustrate the different command trajectories available at $x_0 = 600$ ft. Unlike single impulse results, there is no identifiable trend in the various velocity components. Furthermore, when compared to single impulse results, the total velocity change of the chase vehicle increases nearly an order-of-magnitude. Physically, this indicates that greater fuel expenditure is required to perform the two impulse command trajectories.

However, examining all the above figures reveal that there is a visible trend change at $t_i = 4000$ seconds (~ 66.67 minutes). These trends correspond closely with the changes in the gate and target times for the chase vehicle depicted in Fig. (4.6). This figure shows that the second impulse times are exactly equal to the gate times, t_{gate}. In other words, within this region, Eqn. (4.4) is active. Other adverse results are also visible. First, the performance gradually decreases, i.e. greater positional accuracy is required of the chase vehicle. Second, the second impulse velocity components and magnitude gradually approach zero, i.e. the initial impulse begin to dominate. Thus, based on these indicators, it is fairly safe to surmise that for larger second impulse times the two impulse command trajectory results gradually approach single impulse command trajectory results.

4.2.2   Simulation Results

While Figs. (4.1) - (4.5) illustrate the various command trajectories for $x_0 = 600$ ft, it may be desirable to determine the best overall two impulse command trajectory. At $x_0 = 600$ ft, this would appear to occur at approximately $t_i = 3000$ seconds (50 minutes). This assessment is based on considering both the cost performance and the required ΔV. Based on Figs. (4.1) and (4.5), the performance is 0.731 in with a ΔV of 1.26 in/s. Clearly, the ΔV is not the absolute lowest but is a fairly good estimate of the local minimum given a desired high performance.

34
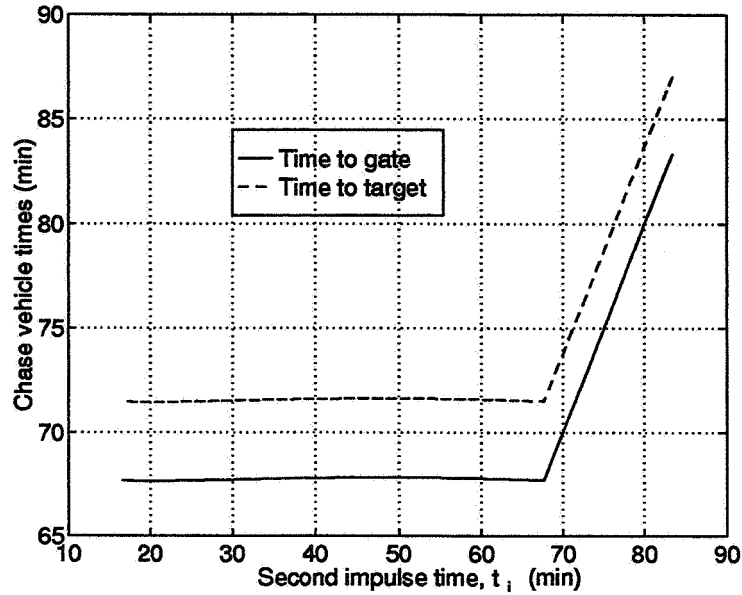
Figure 4.6: Gate and target times for upper trajectories at $x_0 = 600$ ft

Figures (4.7), (4.8), (4.9), and (4.10) are the trajectory simulation results for initial conditions of $x_0 = 600$ ft and $t_i = 3000$ seconds. When compared to single impulse results, two impulse simulations do not appear much different. However, the final approach trajectories do appear to be slightly different than the approach trajectories for the single impulse simulations at $x_0 = 600$ ft. Furthermore, when examining Fig. (4.10), the initial change in the relative vertical position of the chase vehicle is much more abrupt than results obtained in Chapter 3. This would indicate that the vertical component of the initial impulse is greater in magnitude for the two impulse command trajectory. Finally, also note that the total transfer time for the two impulse command trajectory is considerably less than the single impulse command trajectory.

Figure 4.7: Two impulse simulation for chase vehicle starting at $x_0 = 600$ ft with a second impulse time of 3000 seconds

Figure 4.8: Two impulse final approach trajectories for the chase vehicle starting at $x_0 = 600$ ft with a second impulse time of 3000 seconds

Figure 4.9: Horizontal relative position for chase vehicle starting at $x_0 = 600$ ft with a second impulse time of 3000 seconds
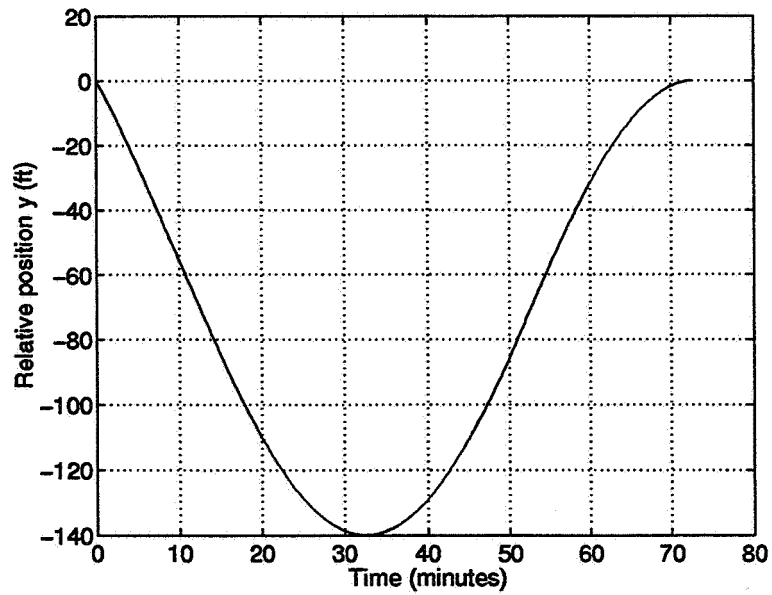
Figure 4.10: Vertical relative position for chase vehicle starting at $x_0 = 600$ ft with a second impulse time of 3000 seconds

As a comparison for other two impulse maneuvers, Figs. (4.11) - (4.13) and Figs. (4.14) - (4.16) simulate command trajectories at second impulse times of 1000 seconds ($\sim$ 16.67 minutes) and 5000 seconds ($\sim$ 83.33 minutes), respectively.

Simulation results for $t_i = 1000$ seconds show a very abrupt change in the optimal chase vehicle trajectory at the second impulse firing. This corresponds with earlier results indicating that the second impulse velocity components dominate the required velocity change for the chase vehicle at early second impulse firings. Furthermore, Fig. (4.13) reveal that the chase vehicle trajectory propagates to relatively lower positions than earlier simulation results. Finally, it is important to note that while these particular results are different than simulation results at $t_i = 3000$ seconds, the performance values between the two simulations are nearly equivalent.

Examination of Figs. (4.14) - (4.16) reveal that simulation results for $t_i = 5000$ seconds are similar to results obtained for a single impulse maneuver. This clearly implies that two impulse command trajectories approach single impulse command trajectories as t_i increases.
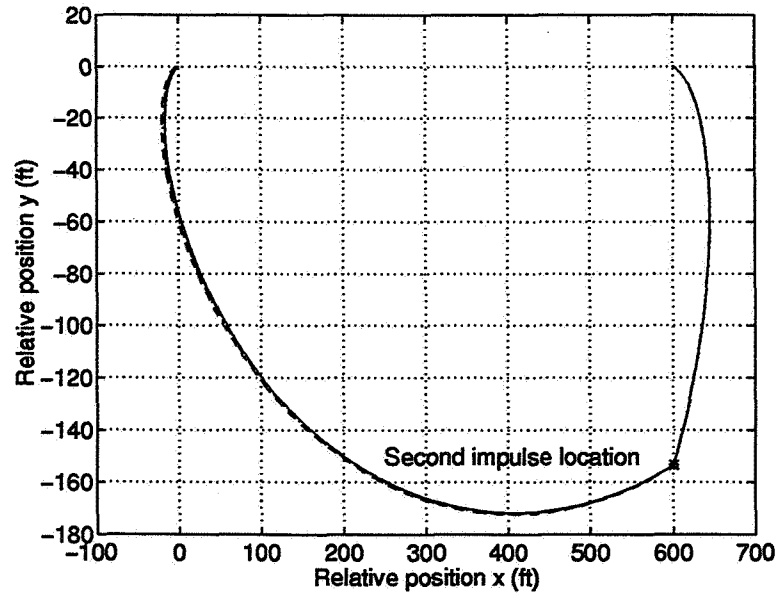
Figure 4.11: Two impulse simulation for chase vehicle starting at $x_0 = 600$ ft with a second impulse time of 1000 seconds
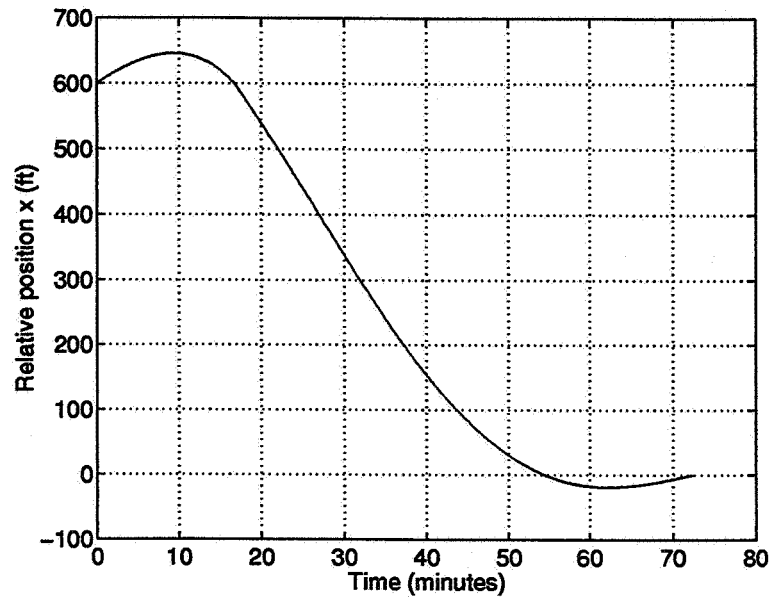
Figure 4.12: Horizontal relative position for chase vehicle starting at $x_0 = 600$ ft with a second impulse time of 1000 seconds
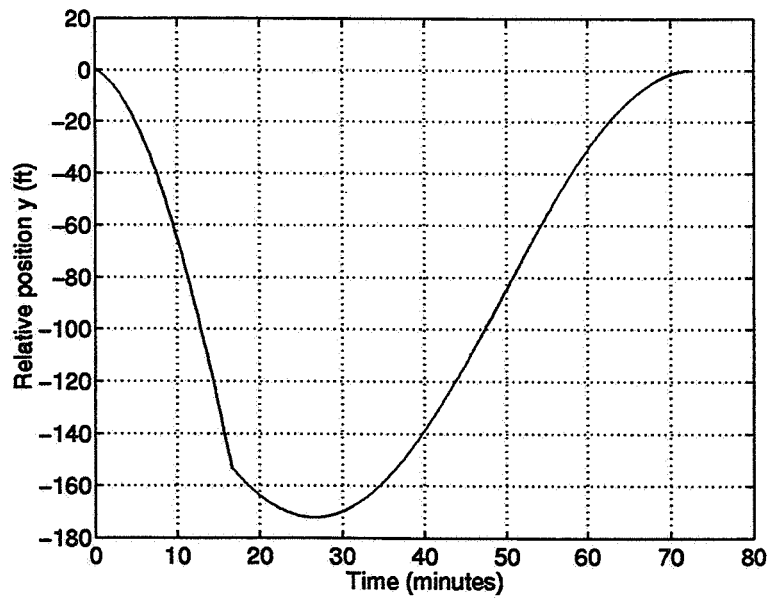
Figure 4.13: Vertical relative position for chase vehicle starting at $x_0 = 600$ ft with a second impulse time of 1000 seconds

39
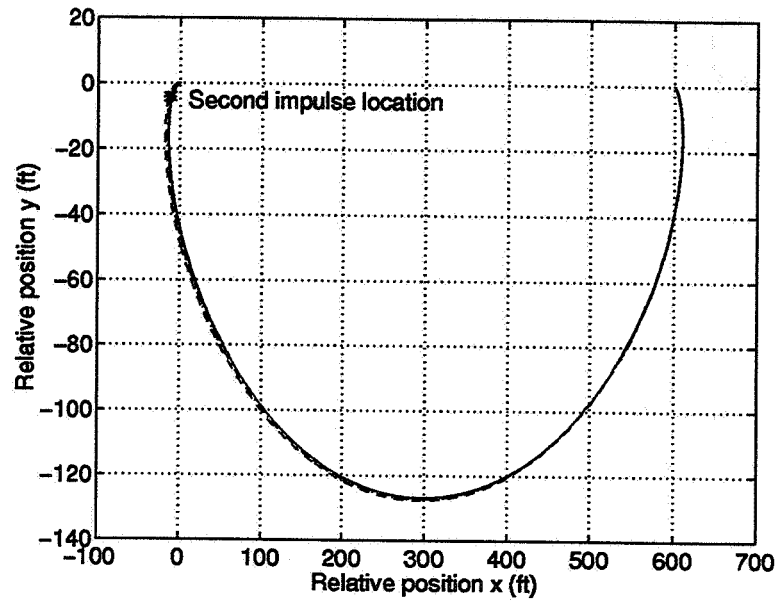
Figure 4.14: Two impulse simulation for chase vehicle starting at $x_0 = 600$ ft with a second impulse time of 5000 seconds
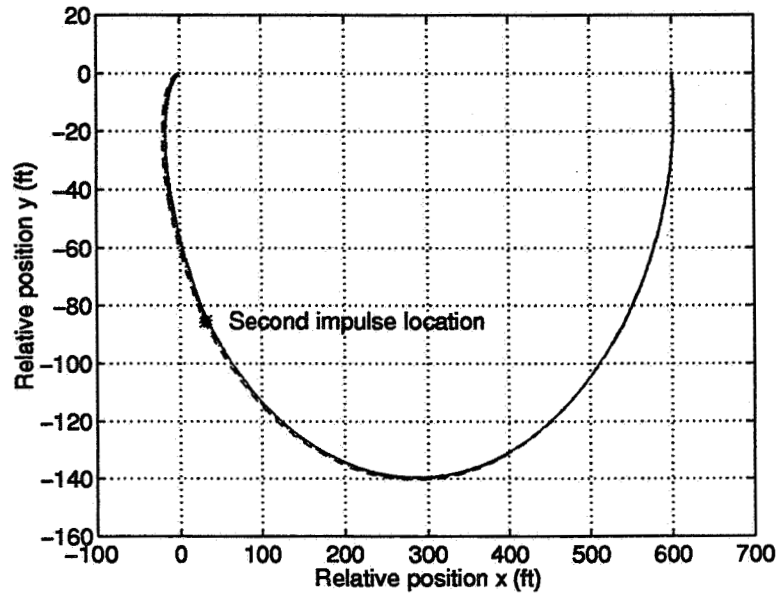

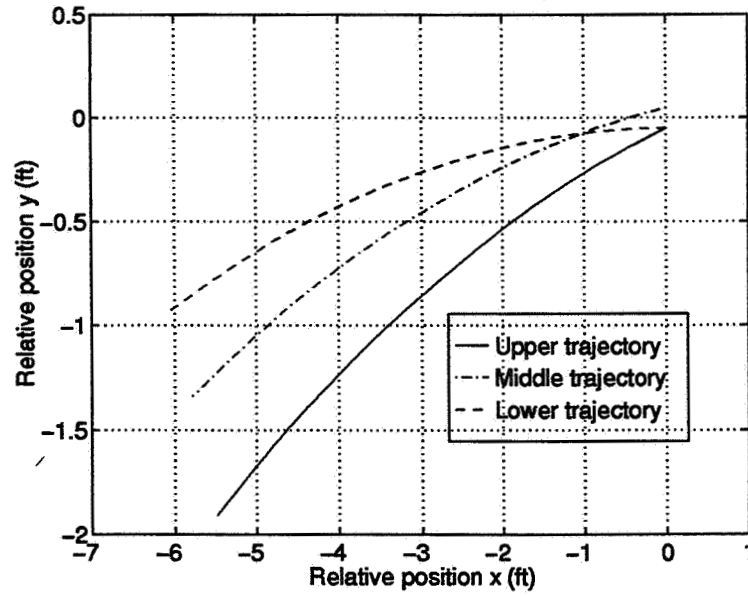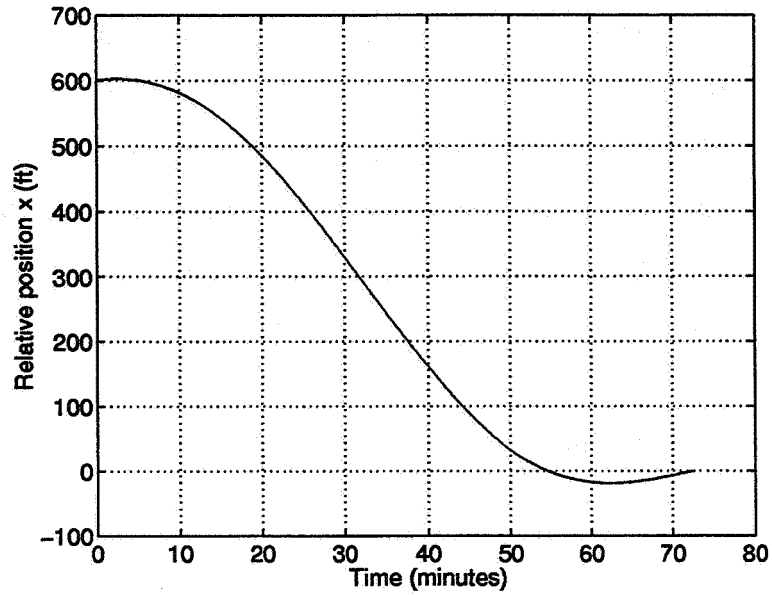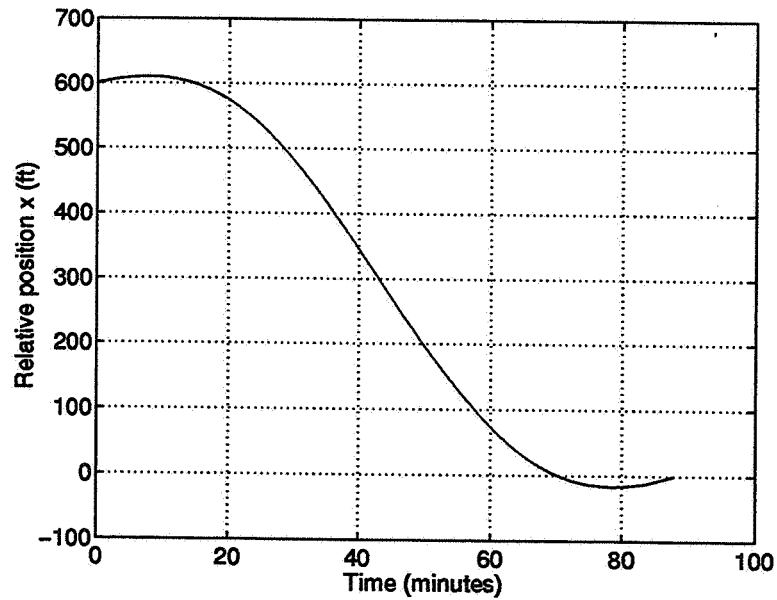Figure 4.15: Horizontal relative position for chase vehicle starting at $x_0 = 600$ ft with a second impulse time of 5000 seconds
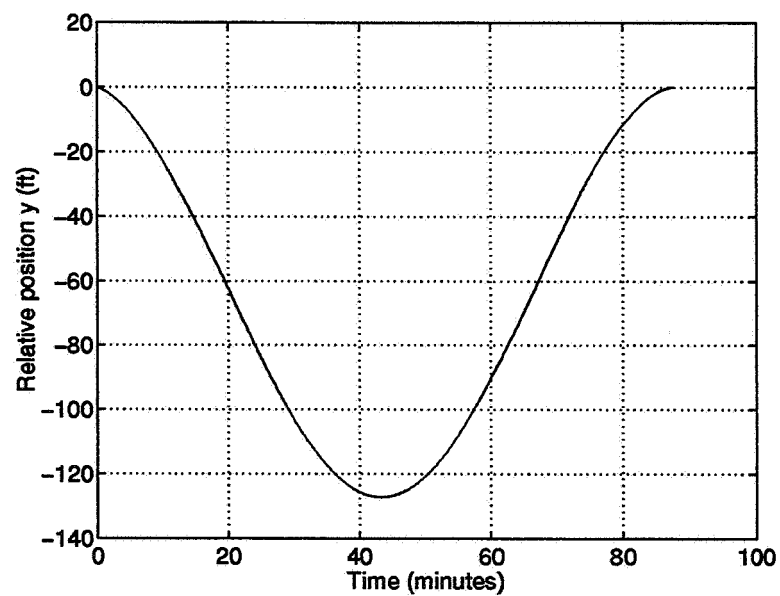
Figure 4.16: Vertical relative position for chase vehicle starting at $x_0 = 600$ ft with a second impulse time of 5000 seconds

Chapter 5

Three Impulse AR&D Maneuver

Results from the two impulse AR&D command trajectory suggest that two impulse maneuvers can provide a viable solution to the terminal phase rendezvous and docking problem presented in this study. However, for the three impulse command trajectory, the performance may be improved by the addition of up to three degrees-of-freedom due to the parameters defining the third impulse. These additional parameters are $\dot{x}_{ii}$, the horizontal velocity component of the third impulse, $\dot{y}_{ii}$, the vertical velocity component of the third impulse, and t_{ii}, the application time of the third impulse. In the results generated for the three impulse command trajectories, the parameters x_0, t_i, and t_{ii} are selected by the user. For each constrained trajectory, the free parameters are x_0, y_0, Δy_0, $\dot{x}_0$, $\dot{y}_0$, $\dot{x}_i$, $\dot{y}_i$, $\dot{x}_{ii}$, $\dot{y}_{ii}$, t_i, t_{ii}, $(t_{targ})_y$, and $(t_{gate})_y$. For a simpler notation, the parameters are defined as

$$\mathcal{F}_3(y) = \{y, (t_{targ})_y, (t_{gate})_y, \dot{x}_0, \dot{y}_0, \dot{x}_i, \dot{y}_i, \dot{x}_{ii}, \dot{y}_{ii}\,;\, x_0, t_i, t_{ii}\} \qquad (5.1)$$

where $y \,\epsilon\, \mathcal{Y}_0$ and $\mathcal{Y}_0$ is defined in Eqn. (3.1).

5.1 Optimization Formulation

The three impulse problem formulation is to maximize Eqn. (3.2) subject to Eqn. (3.18) and

42

$$
\left.
\begin{array}{l}
\mathcal{C}_{gate}(\mathcal{F}_3(y_0 + \Delta y_0)) \\[4pt]
\mathcal{C}_{gate}(\mathcal{F}_3(y_0)) \\[4pt]
\mathcal{C}_{gate}(\mathcal{F}_3(y_0 - \Delta y_0)) \\[4pt]
\mathcal{C}_{targ}(\mathcal{F}_3(y_0 + \Delta y_0)) \\[4pt]
\mathcal{C}_{targ}(\mathcal{F}_3(y_0)) \\[4pt]
\mathcal{C}_{targ}(\mathcal{F}_3(y_0 - \Delta y_0))
\end{array}
\right\}
\tag{5.2}
$$

An additional set of time constraints are also required. These constraints insure the proper and successive firings of the second and third impulses. Since impulse times are user-defined parameters, the additional constraint requires that the time of the third impulse firing, t_{ii}, occurs before the chase vehicle reaches the gate constraint. The following equation represents this condition.

$$
\mathcal{C}_{time_2} = \left\{ \; t_{ii} \le t_{gate} \right.
\tag{5.3}
$$

Since the three trajectory, quadratic-fit formulation is being utilized, Eqn. (5.3) imposes the following set of constraints to the problem statement

$$
\left.
\begin{array}{l}
\mathcal{C}_{time_2}(\mathcal{F}_3(y_0 + \Delta y_0)) \\[4pt]
\mathcal{C}_{time_2}(\mathcal{F}_3(y_0)) \\[4pt]
\mathcal{C}_{time_2}(\mathcal{F}_3(y_0 - \Delta y_0))
\end{array}
\right\}
\tag{5.4}
$$

As with the two impulse command trajectory formulation, these constraints also help to control possible plume impingement.

5.2   Three Impulse AR&D Results

To compare between the various impulse command trajectories, the initial horizontal separation, x_0, is set at 600 ft. Thus, a "3-D" family of results is generated dependent upon t_i and t_{ii}.

The overall effectiveness of the three impulse command trajectory is the enhancement, if any, in the performance of the problem. Figure (5.1) illustrates the scalar

cost function based on varying the second and third impulse times. In this representation, the second impulse firing times range from 1000 seconds after the initial impulse to 3050 seconds after the initial impulse while the third impulse firing times range from 2000 seconds after the initial impulse to 4100 seconds after the initial impulse. Clearly, not all possible solutions are represented in this Fig. (5.1). Due to the extreme complexity of the problem, determining all possible command trajectories based on impulse times is beyond the scope of this study. However, Fig. (5.1) does provide a fairly decent representation of the type of solutions generated by the three impulse optimization problem. Closer examination of Fig. (5.1) reveal that navigational robustness results are similar to the comparable results generated by the two impulse command trajectory. In fact, no significant improvement in the cost function is achieved by implementing a three impulse command trajectory.

A clearer view of the similarity between the three impulse solutions and the two impulse solutions is seen in Fig. (5.2). This illustration is essentially the same as Fig. (5.1) except it is seen from the third impulse time axis. As seen from this particular orientation, the solution to the three impulse optimization formulation is essentially the same as the two impulse formulation. A further comparison of the two command trajectories appear to indicate that the behavior of Δy_0 is highly dependent upon the final impulse and not on the previous impulse firings.
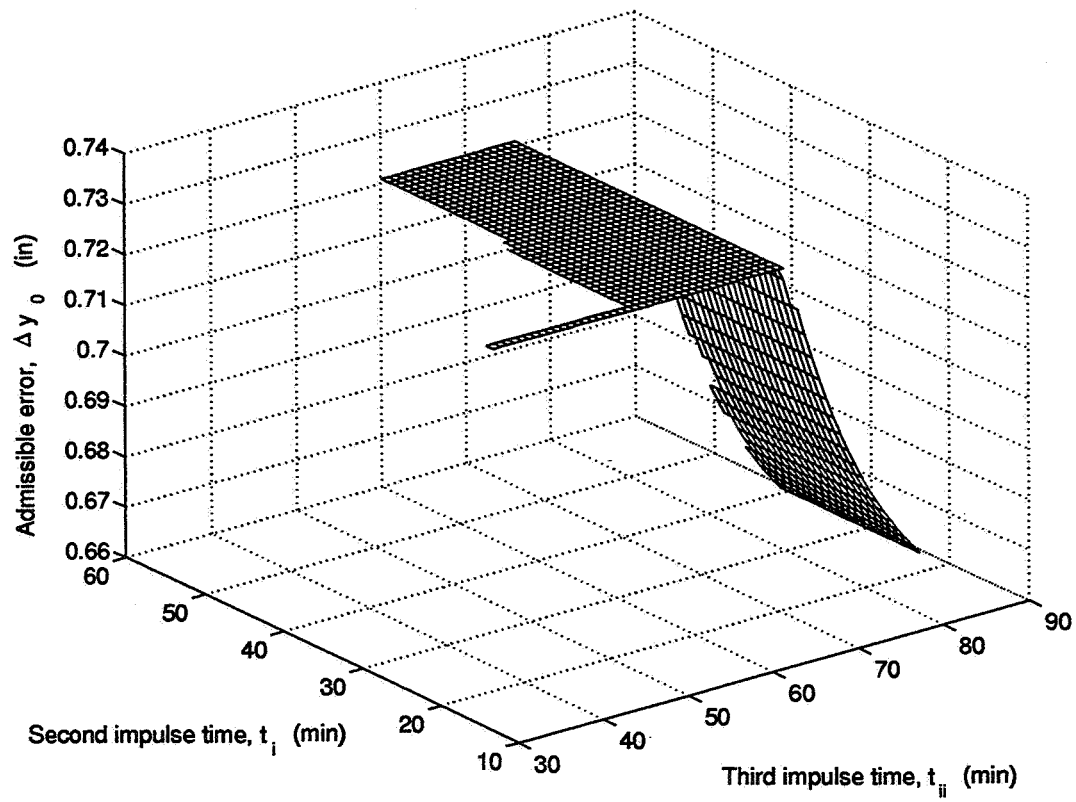
Figure 5.1: Performance robustness with respect to second and third impulse times at $x_0 = 600$ ft
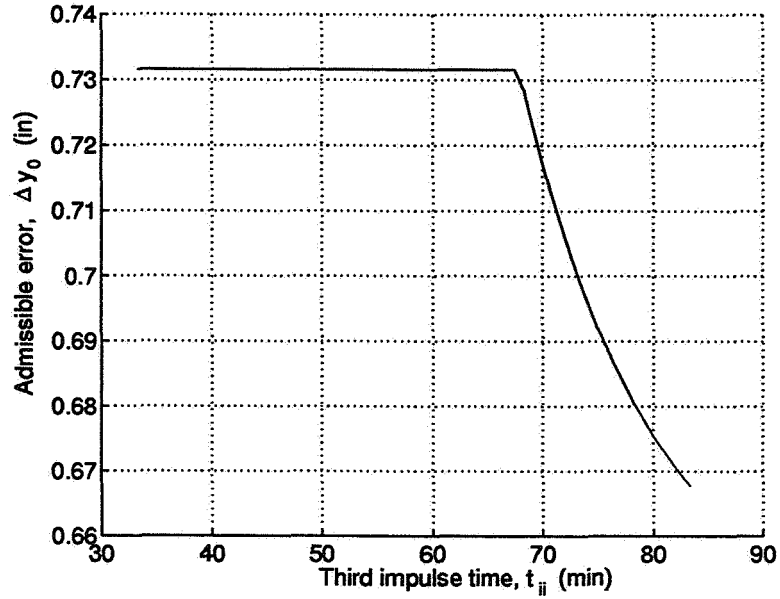
Figure 5.2: Performance robustness with respect to third impulse times

However, while the increase in performance is insignificant, the ΔV experienced by the chase vehicle in the three impulse command trajectory is extreme. Table (5.1) places the slight increase in performance obtained by the three impulse command trajectory in perspective by comparing it to similar results generated by the two impulse command trajectory. In the tabulated results, both schemes are initiated with the chase vehicle starting at 600 ft behind the target vehicle. The two impulse command trajectory results are based on a second impulse firing time of 1000 seconds after the initial impulse while the three impulse command trajectory results are based on second and third impulse firing times of 1000 seconds and 2020 seconds after the initial impulse, respectively. While the performance has a marginal increase of 0.41%, the total ΔV required of the chase vehicle increases by 49.88%. Thus, the implementation of a three impulse command trajectory over a two impulse command trajectory is not warranted when considering the subsequent increase in fuel cost in relation to the slight improvement in performance.

Table 5.1: Percent increase comparisons between the two impulse command trajectory and the three impulse command trajectory

	Two impulse	Three impulse	% change
Δy_0 (in)	0.728	0.731	+0.41%
ΔV_0 (in/s)	1.61	0.118	-92.67%
ΔV_i (in/s)	2.46	4.27	+73.57%
ΔV_{ii} (in/s)	N/A	1.71	N/A
ΔV (in/s)	4.07	6.10	+49.88%

Chapter 6

Thruster Management System

Recall from Chapter 1 that the assumed guidance architecture is an open-loop system utilizing relative GPS for initial position determination. While previous chapters detail the work in determining optimized command trajectories, this chapter examines the preliminary steps taken to complete the guidance architecture.

6.1 Cargo Transfer Vehicle (CTV)

The first step in designing the thruster management system is to determine the reference design for the chase vehicle. The reference design utilized for the AR&D simulations will be NASA's cargo transfer vehicle (CTV). The CTV has an empty mass of 308.1 slugs and has twenty-four 11.24 lbf thrusters. These thrusters are used for orbit transfer and attitude control. Table (6.1) lists the normalized force vector and the thruster location with respect to the CTV origin while Table (6.2) lists the CTV and payload mass properties (priv. communication - Mr. Richard Dabney, MSFC - Sept. 28, 1994).

The basic concept for the thruster management system is two-fold. Due to the amount of thrusters available on the CTV, optimal throttle settings for each of the thrusters are determined such that the resulting motion is purely translational. In other words, given an impulse command from the command trajectories, theoretical throttle settings are determined such that the desired ΔV is generated with no

48

Table 6.1: CTV thruster location and force vector directions

Thruster	Normalized force vector			Thruster location (ft)		
1	1.00	0.00	0.00	-9.84	4.66	4.66
2	1.00	0.00	0.00	-9.84	4.66	-4.66
3	1.00	0.00	0.00	-9.84	-4.66	-4.66
4	1.00	0.00	0.00	-9.84	-4.66	4.66
5	0.00	1.00	0.00	-9.84	-4.66	4.66
6	0.00	1.00	0.00	-9.84	-4.66	-4.66
7	0.00	1.00	0.00	0.00	-4.66	-4.66
8	0.00	1.00	0.00	0.00	-4.66	4.66
9	0.00	0.00	1.00	-9.84	4.66	-4.66
10	0.00	0.00	1.00	0.00	4.66	-4.66
11	0.00	0.00	1.00	0.00	-4.66	-4.66
12	0.00	0.00	1.00	-9.84	-4.66	-4.66
13	-0.7071	-0.50	-0.50	-9.84	4.66	4.66
14	-0.7071	-0.50	0.50	-9.84	4.66	-4.66
15	-0.7071	0.50	0.50	-9.84	-4.66	-4.66
16	-0.7071	0.50	-0.50	-9.84	-4.66	4.66
17	0.00	-1.00	0.00	-9.84	4.66	4.66
18	0.00	-1.00	0.00	-9.84	4.66	-4.66
19	0.00	-1.00	0.00	0.00	4.66	-4.66
20	0.00	-1.00	0.00	0.00	4.66	4.66
21	0.00	0.00	-1.00	-9.84	4.66	4.66
22	0.00	0.00	-1.00	0.00	4.66	4.66
23	0.00	0.00	-1.00	0.00	-4.66	4.66
24	0.00	0.00	-1.00	-9.84	-4.66	4.66

Table 6.2: CTV and payloads mass properties

	Mass (slugs)	I_{xx} (slugs-ft^2)	I_{yy} (slugs-ft^2)	I_{zz} (slugs-ft^2)
Empty CTV	308.1	57.24	50.09	50.09
Propellants	308.1	32.20	37.57	37.57
Payload 1	855.8	159.0	185.5	185.5
Payload 2	1712	318.0	371.0	371.0
Payload 3	1712	318.0	1007	1007

resultant moment experienced by the CTV. However, since most thrusters used in space are not throttlable, the second part of the control system involves developing a modulator which uses the optimal throttle settings to determine the minimum firing times for each of the thrusters.

In designing the thruster management system for the CTV, this study focuses upon developing the formulations for determining optimal throttle settings given desired impulse commands. Completing the thruster management system would simply involve developing a modulator to determine minimum firing times and a trajectory correction mechanism to account for non-impulsive motion. No effort was made in developing the modulator or trajectory correction mechanism.

6.2 Thruster Firing Concept

In terms of control, probably the most difficult issue to handle is not the translational motion of the vehicle but rather the rotational motion and the ensuing rotational dynamics associated with such a motion. Since the two impulse command trajectory assumes a point mass with no rotational dynamics, it would be desirable to implement a thruster management system which determines the optimal thruster firings for pure translational motion given a desired ΔV. In many vehicle configurations, it would probably not be possible to utilize such a control scheme but since the CTV model consists of twenty-four thrusters (twice the amount theoretically required for 6-DOF),

a thruster management concept in this manner should be possible regardless of the type of ΔV required by the command trajectory.

6.2.1 Formulations for Optimal CTV Thruster Firings

The thruster management concept is based on determining the minimum theoretical throttle settings for each thruster to accomplish the inputted guidance commands such that no rotational motion results from the thruster firings. Since throttle settings must be positive values, the mathematical model for each of the thrusters are represented as

$$\vec{T}_j = a_j{}^2 \vec{e}_j \tag{6.1}$$

where $j = 1, 2, \ldots, 24$, $\vec{e}$ represent the normalized force vectors for each thruster, and a_j^2 represent the throttle setting ranging from zero to one.

The scalar cost function is to minimize the sum of all the thruster magnitudes. This is the equivalent to stating that

$$
\begin{aligned}
\mathcal{J} &= \sum_{j=1}^{24} \{|\vec{T}_j|^2\} \\
&= \sum_{j=1}^{24} \{a_j^4 |\vec{e}_j|^2\}
\end{aligned}
\tag{6.2}
$$

However, since the normalized force directions are unit vectors, the magnitude of $\vec{e}$ is simply equal to one. Thus, the cost function can be simplified to the following

$$\mathcal{J} = \sum_{j=1}^{24} a_j^4 \tag{6.3}$$

The scalar cost function is constrained to two criteria. First, the throttle settings must produce a resultant force vector such that the resulting vehicle motion proceeds in the desired velocity direction. Second, the CTV must move in pure translational motion. Thus, the sum of all the moments generated by the different thrusters must be equal to zero. Mathematically, the constraints can be expressed as the following

51

$$\vec{C_1} = \Delta \vec{V} - \sum_{j=1}^{24} \vec{T_j} = 0 \qquad (6.4)$$

$$\vec{C_2} = \sum_{j=1}^{24} \{\vec{T_j} \times \vec{r_j}\} = 0 \qquad (6.5)$$

It is important to note that while, mathematically, the constraints are represented as two equations, the constraints themselves are vectors which must be zeroed.

6.2.2 Solving the Thruster Firing Optimization Problem

The thruster management problem is solved using a step-restricted Newton-Raphson routine. The routine is implemented to solve the necessary conditions generated by the Lagrangian [13]. The Lagrangian is defined as the following

$$L = \mathcal{J} + \vec{\lambda_1} \cdot \vec{C_1} + \vec{\lambda_2} \cdot \vec{C_2} \qquad (6.6)$$

The unknowns in this problem are the 24 throttle settings and the Lagrange multiplier vectors. To insure that the throttle settings are always positive, the Newton-Raphson routine solves for the square root of the throttle settings, i.e. a_j. Using (6.6), the necessary conditions are as follows

$$\left. \begin{array}{l} \frac{\partial L}{\partial a_j} = 0 \\[2mm] \frac{\partial L}{\partial \vec{\lambda_1}} = 0 \\[2mm] \frac{\partial L}{\partial \vec{\lambda_2}} = 0 \end{array} \right\} \qquad (6.7)$$

Recalling that the constraints are vector constraints, the throttle optimization formulation requires 30 necessary conditions.

6.2.3 Representative Throttle Setting Results

Figures (6.1) and (6.2) illustrate some representative results for optimal throttle settings given a desired impulse direction. Figure (6.1) display optimal throttle settings when the desired velocity change is in the positive unit axis direction. Likewise, Fig.

(6.2) display optimal throttle settings when the desired velocity change is in the negative unit axis direction. Each individual subplot in the figures represent optimization results from the step-restricted Newton-Raphson routine.
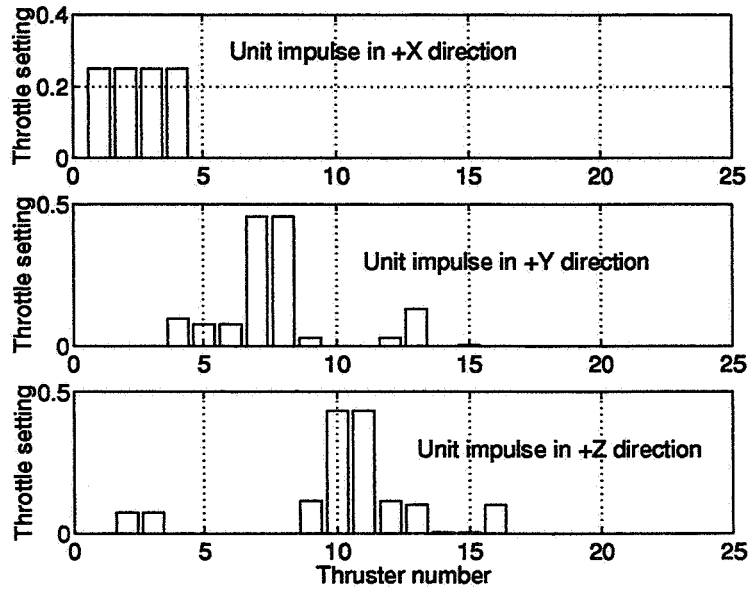
Figure 6.1: Optimal throttle settings for positive axial direction unit impulses
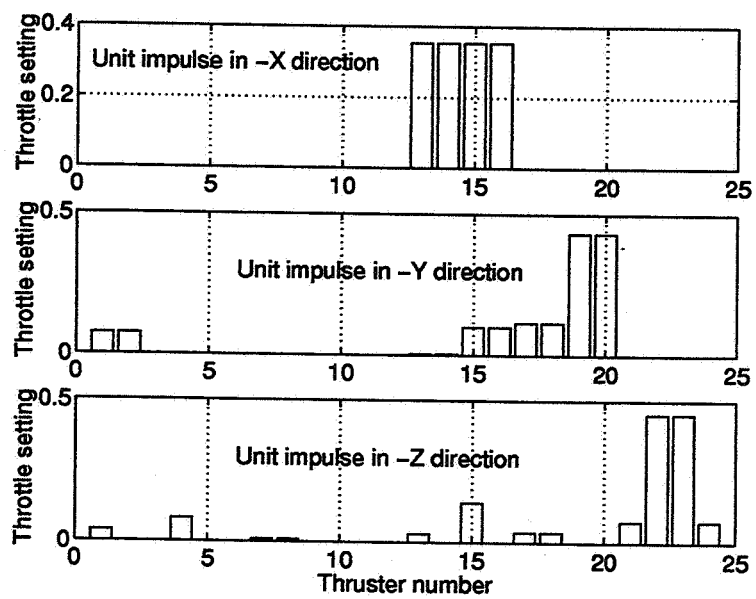
Figure 6.2: Optimal throttle settings for negative axial direction unit impulses

Chapter 7

Summary and Recommendations

This study focused upon the development of an open-loop guidance architecture for the terminal phase of an autonomous rendezvous and docking (AR&D) mission to determine the capability of using the Global Positioning System (GPS) for initial relative position determination instead of conventional optical sensors. The development of the guidance architecture was performed in two steps. First, feasible command trajectories were determined for one, two, and three impulse maneuvers. Second, a thruster management system was developed to execute these command trajectories.

Several assumptions were made concerning the type of terminal phase docking maneuver. First, the chase vehicle was on-orbit with the target and trailed the target by a given distance. Second, while at its initial position, the chase vehicle was assumed to have no relative motion with respect to the target. Third, the docking mechanism was assumed to be located on the far side of the target vehicle. This required a docking maneuver where the chase flies to the front of the target to complete the mission. Finally, relative GPS issues such as integer ambiguity and cycle slip were assumed to be resolved. In this study, linear time-invariant equations of motions were used to govern the relative dynamics between the chase and target vehicles.

Previous command trajectory research suggested that docking accuracies were highly sensitive to initial vertical position errors while fairly insensitive to initial horizontal position errors of the chase vehicle. In this study, command trajectories were deemed feasible by maximizing the locus of admissible initial vertical positions

and comparing the maximum vertical position error to documented relative GPS accuracies. In this study, constrained trajectory optimization was used to determine this locus of initial positions.

Results show that for small initial horizontal separations between the chase and target vehicles, one impulse command trajectories were not feasible based on required initial vertical position accuracy. For small separations, the initial vertical position accuracy were too stringent for relative GPS position determination. The robustness for two impulse command trajectories were significantly better. The accuracy required of two impulse command trajectories were determined to clearly be obtainable using relative GPS. At a given initial horizontal separation, required initial vertical position accuracies were nearly constant regardless of the application time of the second impulse. As compared to two impulse command trajectory results, initial vertical position accuracy requirements for the three impulse command trajectory exhibited no significant improvement. However, the increase in total velocity change required of the chase vehicle was significant to the point where the implementation of a three impulse maneuver over a two impulse maneuver was not warranted. From an engineering standpoint, the two impulse command trajectory was the best maneuver to complete the specified docking mission.

The development of the thruster management system was based upon determining optimal throttle settings given a desired impulse command. In addition to realizing the impulse command, an additional constraint required that the resultant chase vehicle motion was purely translational. The specific model used for the chase vehicle was the cargo transfer vehicle. In this study, it was determined that formulations could be developed where the thruster management system realized the impulse commands while producing no resultant moment. Research in designing the management system was preliminary in that no effort was made on developing a modulator to determine minimum thruster firing times based on the throttle settings.

There are several areas of possible future work in this field. Additional work is required to complete the thruster management system. Future work could also involve examining thruster error and finite-burn effects. Additionally, navigational

errors and pointing errors are very important with these maneuvers. Thus, future research could be devoted to these issues. Other areas of recommended research could involve incorporating other force effect, such as differential drag, gravitational effect of the Moon, and solar pressure, which can affect the desired motion of the chase vehicle. Finally, future work could involve developing a closed-loop guidance, navigation, and control system where navigation corrections are performed by relative GPS in real-time.

Bibliography

[1] Leonard, C. L. and Bergmann, E. V., "A Survey of Rendezvous and Docking Issues and Developments", *Orbital Mechanics and Mission Design: Advances in the Astronautical Sciences*, Vol. 69, Paper AAS 89-158, April 24-27, 1989, pp. 85-101.

[2] Kunkel, B., Lutz, R., and Manhart, S., "Advanced Opto-electrical Sensors for Autonomous Rendezvous-Docking and Proximity Operations in Space", *Proceedings Solid State Imagers and Their Applications*, Vol. 591, Nov. 26-27, 1985, pp. 138-148.

[3] Fukase, M., Maruyama, T., Uchiyama, T., Okamoto, O., and Yamaguchi, I., "Visual Sensing for Autonomous Rendezvous and Docking", *41st Congress of the International Astronautical Federation*, Oct. 6-12, 1990.

[4] Curtis, A., ed., *Space Satellite Handbook, 3rd Edition*, Gulf Publishing Company, 1994, pp. 86-87, 114-115.

[5] Green, G. B., Massatt, P. D., and Rhodus, N. W.,"The GPS 21 Primary Satellite Constellation", *Navigation: Journal of the Institute of Navigation*, Vol. 36, No. 1, Spring 1989, pp. 9-24.

[6] Upadhyay, T., Cotterill, S., and Deaton, A. W., "Autonomous Reconfigurable GPS/INS Navigation and Pointing System for Rendezvous and Docking", *AIAA Space Programs and Technologies Conference*, March 24-27, 1992.

[7] Hohwiesner, B. and Pairot, J., "On-Orbit Demonstration of Automated Closure and Capture Using European & NASA Proximity Operations Technologies

and an Existing, Serviceable NASA Explorer Platform Spacecraft", *AIAA Space Programs and Technologies Conference*, March 24-27, 1992.

[8] Smith, A., Hesper, E., Kuijper, D., Mets, G., Ambrosius, B., and Wakker, K., "TOPEX/Poseidon Precise Orbit Determination", *Spaceflight Mechanics 1994*, Vol. 87, Part II, Paper AAS 94-137, 1994, pp. 1107-1124.

[9] Euler, H., "Achieving High-Accuracy Relative Positioning in Real-time: System Design, Performance and Real-time Results", *1994 IEEE Position Location and Navigation Symposium*, April 11-15, 1994, pp. 540-546.

[10] DiPrinzio, M.D. and Tolson, R.H., "Evaluation of GPS Position and Attitude Determination for Automated Rendezvous and Docking Missions", *NASA Contractor Report 4614*, July 1994.

[11] Mullin, L.D., "Initial Value and TPBV Solutions to the Clohessy-Wiltshire Equations", *The Journal of Astronautical Sciences*, Vol. 40, No. 4, Oct.-Dec. 1992, pp. 487-501.

[12] Burden, R. L. and Faires, J. D., *Numerical Analysis, Fifth Edition*, PWS-Kent Publishing Company, 1993, pp. 98-105.

[13] Bryson, A. E. and Ho, Y., *Applied Optimal Control: Optimization, Estimation, and Control*, Hemisphere Publishing Corporation, 1975.

Appendix A

Early AR&D Formulations

The optimization formulations and results presented in this appendix illustrate early, unpublished AR&D research performed by Dr. Daniel D. Moerder (NASA LaRC) and Dr. Robert B. Bless (Lockheed). The basic research involves determining optimized trajectories for a single impulse command trajectory with no preconceptions about the initial position error sensitivities in relation to docking accuracies. Thus, their formulations involve determining a locus of initial positions, x_0 and y_0, and not just a locus of initial vertical positions. Within this locus, the chase vehicle performs a fixed sequence of impulses which translates the vehicle into the target while satisfying the accuracy requirements listed in Table (2.1).

A.1 Early AR&D Problem Statement

An early approach to this problem is to determine the maximum two-dimensional "footprint" of admissible initial positions for the chase vehicle such that a single fixed impulse anywhere within this footprint results in a successful docking with the target.

In polar coordinates, the formulation is to maximize

$$\mathcal{J} = x_0^2 + y_0^2 = r_0^2 \qquad \text{(A.1)}$$

where the initial position is represented as

$$\left. \begin{array}{rcl} x_0 & = & r_0 \cos\theta \\ y_0 & = & r_0 \sin\theta \end{array} \right\} \qquad \text{(A.2)}$$

To generate a footprint of admissible initial positions, the parameter θ is allowed to range from 0 deg to 360 deg. In this approach, the only constraints to the optimization problem are to satisfy the target conditions summarized in Table (2.1) and represented mathematically in Eqn. (2.4).

A.2 Early AR&D Results

Figure (A.1) illustrate admissible position errors about the nominal initial chase vehicle position, x_0 and y_0, which in this figure is centered about the origin. These AR&D results show that to meet the accuracy required at docking the position errors of the chase vehicle at its initial condition are very sensitive to the initial vertical position errors while fairly insensitive to horizontal position errors. In fact, the admissible errors in the horizontal position of the chase vehicle are in the order-of-magnitude of several feet. Documented results of relative GPS orbit determination performance has demonstrated that local horizontal position errors of several feet are clearly obtainable [8, 9, 10]. However, based purely on these results, it is uncertain whether the admissible errors in the initial vertical position of the chase vehicle is attainable through relative GPS position determination.

It is important to point out that this early AR&D formulation is based on the assumption that intermediate trajectories within the boundary of the footprint satisfy target constraints. However, results from Chapter 3 show that this assumption is not true without actually constraining the interior trajectories. Thus, if interior trajectory constraints are included in the formulation, the overall magnitude of the footprint
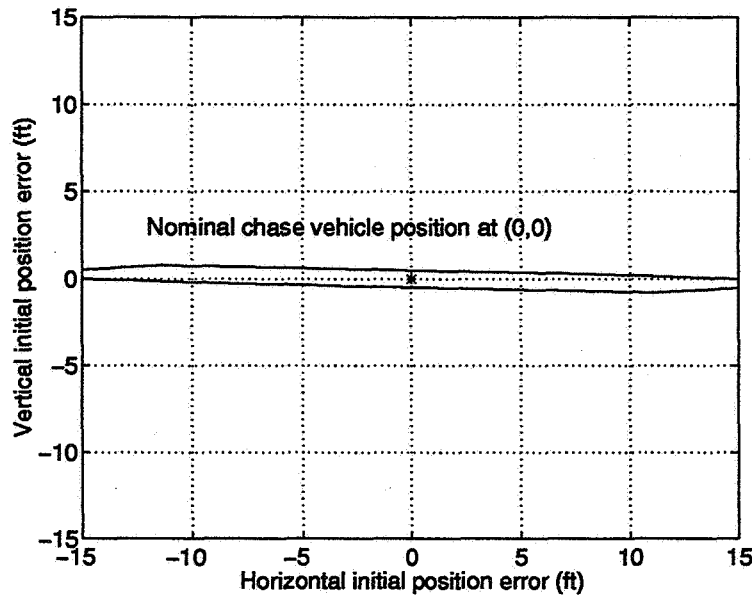
Figure A.1: Early AR&D footprint results of admissible position errors at the chase vehicle initial condition

would decrease, but it is safe to presume that the trend exhibited in Fig. (A.1) would continue to exist.

Furthermore, optimized trajectory simulations of this single impulse AR&D maneuver are performed based on the optimization formulation of Eqns. (A.1) and (2.4). Figure (A.2) illustrate two chase vehicle trajectories initiated from the uppermost and lowermost admissible vertical positions. Based on Fig. (A.2), the chase vehicle approaches the target vehicle tangentially from either side. In this basic formulation, the final approach trajectory of the chase vehicle is uncontrolled. Ideally, it is best to formulate the trajectory optimization problem such that the chase vehicle always approaches the target from a specified direction. As seen in Fig. (A.2), to accommodate different chase vehicle approach trajectories, the target vehicle docking port would have to be continually reorientated based upon the initial position of the chase vehicle. While reorientating small target vehicles would certainly be possible, this scenario is impractical for large proposed target structures such as Space Station Freedom.
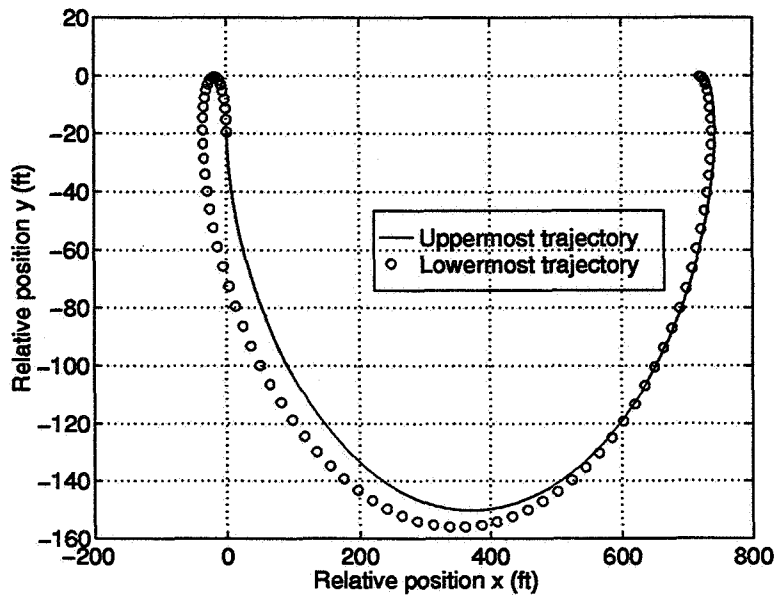
Figure A.2: Early AR&D trajectory simulation starting from the extreme ends of admissible initial vertical chase positions

The results of this early AR&D formulation lay the groundwork for the current constrained trajectory optimization problem presented in Chapter 3. It hints at the need to maximize a locus of initial vertical positions for the chase vehicle. It also illustrates the required addition of gate constraints that must be satisfied by the chase vehicle to generate more direct and predictable optimized approach trajectories.

Appendix B

Quadratic Behavior at Target Vehicle

Analysis of rendezvous and docking results has shown that Eqn. (3.5) is violated for the intervals of $y_0 - \Delta y_0 \leq y_0 \leq y_0 + \Delta y_0$ at a given x_0. To adequately satisfy this constraint, an assumed parabolic behavior of e_y is exploited by modeling the behavior of Eqn. (3.5) as a quadratic according to Eqn. (3.16). The additional constraint expression of Eqn. (3.18) is required in the three trajectory problem formulation.

There are two governing equations related to the behavior of y_f. By the Clohessy-Wiltshire dynamical model [11], they are

$$x(y_0, t) = x_0 + 6y_0(\omega t - \sin \omega t) + \dot{x}_0(\frac{4 \sin \omega t}{\omega} - 3t) + \frac{2\dot{y}_0}{\omega}(1 - \cos \omega t) \qquad (B.1)$$

$$y(y_0, t) = (4 - 3\cos \omega t)y_0 - \frac{2\dot{x}_0}{\omega}(1 - \cos \omega t) + \frac{\dot{y}_0}{\omega}\sin \omega t \qquad (B.2)$$

where x_0, $\dot{x}_0$, and $\dot{y}_0$ are assumed to be given for a particular command trajectory.

To show quadratic behavior, Eqns. (B.1) and (B.2) are expanded about the target, i.e. at $t = t_f$, using a first-order Taylor series. The Taylor series will have the form:

$$\delta x_f = \frac{\partial x(y_0, t_f)}{\partial t_f}\delta t_f + \frac{\partial x(y_0, t_f)}{\partial y_0}\delta y_0 + H.O.T \qquad (B.3)$$

64

$$\delta y_f = \frac{\partial y(y_0, t_f)}{\partial t_f} \delta t_f + \frac{\partial y(y_0, t_f)}{\partial y_0} \delta y_0 + H.O.T \qquad (B.4)$$

where, at the target, $\delta x_f = 0$. Note that the higher-order terms in Eqns. (B.3) and (B.4) are negligible since secular terms exist in the governing equations.

From Eqn. (B.3), a set of all feasible solutions of δt_f in terms of δy_0 is found to be

$$\delta t_f = \frac{6(\sin \omega t_f - \omega t_f)}{6 \omega y_0 (1 - \cos \omega t_f) - \dot{x}_0 (3 - 4 \cos \omega t_f) + 2 \dot{y}_0 \sin \omega t_f} \delta y_0 \qquad (B.5)$$

Using Eqns. (B.4) and (B.5), a perturbation relation between δy_f and δy_0 is found to be of the form:

$$\frac{\delta y_f}{\delta y_0} = \frac{A y_0 + B}{C y_0 + D} \qquad (B.6)$$

where

$$\left. \begin{aligned}
A &= 6\omega(7 - 7\cos \omega t_f - 3\omega t_f \sin \omega t_f) \\
B &= \dot{x}_0(12\omega t_f \sin \omega t_f + 25 \cos \omega t_f - 24) + \dot{y}_0(8 \sin \omega t_f - 6\omega t_f \cos \omega t_f) \\
C &= 6\omega(1 - \cos \omega t_f) \\
D &= \dot{x}_0(4 \cos \omega t_f - 3) + 2\dot{y}_0 \sin \omega t_f
\end{aligned} \right\} \qquad (B.7)$$

Recall that Eqn. (B.7) contains x_0, $\dot{x}_0$, and $\dot{y}_0$ which are assumed to be given for a particular impulse scheme.

Clearly, the perturbation relation of Eqn. (B.6) represent the tangential relationship between the final position of the chase vehicle, y_f, in terms of its initial position, y_0. To show a relation is quadratic with a clear maximum point is the equivalent to showing that the corresponding tangential relation is linear. The relation derived using perturbation methods is a ratio of linear relations for all feasible solutions of t_f and y_0. However, results for the impulse command trajectories posed in this work consist of a specific set of feasible solutions. Thus, to show that Eqn. (B.6) is linear, the magnitude of A must dominate the magnitude of C. Evaluating Eqn. (B.7) using

optimized single impulse solutions at $x_0 = 600$ ft results in the following order of magnitudes:

$$\left.\begin{array}{l} A \approx 10^{-2} \\ B \approx 10^{-1} \\ C \approx 10^{-5} \\ D \approx 10^{-2} \end{array}\right\} \tag{B.8}$$

Based on Eqn. (B.8), the dominant linear relation in Eqn. (B.6) is the numerator. The dominant term in the denominator of Eqn. (B.6) is the stand-alone constant D. In fact, the smallest order of magnitude in Eqn. (B.8) is the one associated with the linear coefficient term in the denominator. At $O(10^{-5})$, this term is three orders-of-magnitude smaller than the magnitude of A which clearly implies that Eqn. (B.6) can be approximated as a linear relation. Figure (B.1) displays Eqn. (B.6) using results from the optimized single impulse command trajectory over the entire interval of y_0 and its corresponding set of t_f. The graphic shows a decreasing linear relation crossing the zero axis. This shows fairly conclusively that $y_f(y_0)$ is a parabolic relation with a clear maximum.
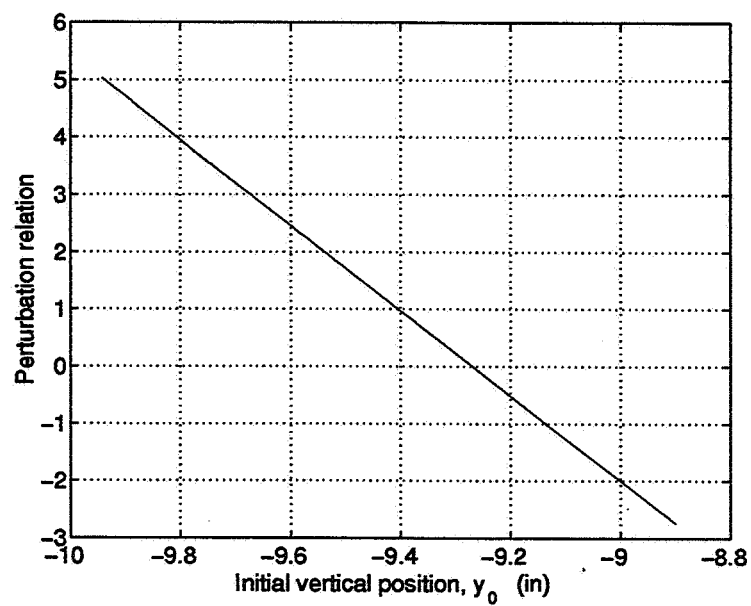
Figure B.1: Perturbation results of $\frac{\delta y_f}{\delta y_0}$ using optimized single-impulse results at x_0=600 ft

REPORT DOCUMENTATION PAGE

Public reporting burden for this collection of information is estimated to average 1 hour per response, including the time for reviewing instructions, searching existing data sources, gathering and maintaining the data needed, and completing and reviewing the collection of information. Send comments regarding this burden estimate or any other aspect of this collection of information, including suggestions for reducing this burden, to Washington Headquarters Services, Directorate for Information Operations and Reports, 1215 Jefferson Davis Highway, Suite 1204, Arlington, VA 22202-4302, and to the Office of Management and Budget, Paperwork Reduction Project (0704-0188), Washington, DC 20503.

1. AGENCY USE ONLY (Leave blank)	2. REPORT DATE	3. REPORT TYPE AND DATES COVERED
	August 1995	Contractor Report

4. TITLE AND SUBTITLE

An Open Loop Guidance Architecture For Navigationally Robust On-orbit Docking

5. FUNDING NUMBERS

NCC1-104

WU 242-80-01-02

6. AUTHOR(S)

Hung-Sheng Chern

7. PERFORMING ORGANIZATION NAME(S) AND ADDRESS(ES)

The George Washington University
Joint Institute for Advancement of Flight Sciences
NASA Langley Research Center
Hampton, VA 23681-0001

8. PERFORMING ORGANIZATION REPORT NUMBER

9. SPONSORING / MONITORING AGENCY NAME(S) AND ADDRESS(ES)

National Aeronautics and Space Administration
Langley Research Center
Hampton, VA 23681-0001

10. SPONSORING / MONITORING AGENCY REPORT NUMBER

NASA CR-4687

11. SUPPLEMENTARY NOTES

The information presented in this report was offered as a thesis by the author in partial fulfillment of the requirements for the Degree of Master of Science, The George Washington University, July 1995.
Langley Technical Monitor: Daniel D. Moerder

12a. DISTRIBUTION / AVAILABILITY STATEMENT

Unclassified - Unlimited
Subject Category 18

12b. DISTRIBUTION CODE

13. ABSTRACT (Maximum 200 words)

The development of an open-loop guidance architecture is outlined for autonomous rendezvous and docking (AR&D) missions to determine whether the Global Positioning System (GPS) can be used in place of optical sensors for relative initial position determination of the chase vehicle. Feasible command trajectories for one, two, and three impulse AR&D maneuvers are determined using constrained trajectory optimization. Early AR&D command trajectory results suggest that docking accuracies are most sensitive to vertical position errors at the initial conduction of the chase vehicle. Thus, a feasible command trajectory is based on maximizing the size of the locus of initial vertical positions for which a fixed sequence of impulses will translate the chase vehicle into the target while satisfying docking accuracy requirements. Documented accuracies are used to determine whether relative GPS can achieve the vertical position error requirements of the impulsive command trajectories. Preliminary development of a thruster management system for the Cargo Transfer Vehicle (CTV) based on optimal throttle settings is presented to complete the guidance architecture. Results show that a guidance architecture based on a two impulse manuever generated the best performance in terms of initial position error and total velocity change for the chase vehicle.

14. SUBJECT TERMS

Rendezvous and Docking, On-orbit Maneuvers, Space Vehicle Guidance

15. NUMBER OF PAGES

82

16. PRICE CODE

A05

17. SECURITY CLASSIFICATION OF REPORT	18. SECURITY CLASSIFICATION OF THIS PAGE	19. SECURITY CLASSIFICATION OF ABSTRACT	20. LIMITATION OF ABSTRACT
unclassified	unclassified		